ADVANCED MATERIALS
www.advmat.de

Solvation Chemistry of Nonaqueous Electrolytes for Rechargeable Magnesium Batteries

Juncai Long, Ze He, Ge Zhang, Yao Ding, Jianyong Zhang, Pei Liu, Hantao Xu, Rui Wang, Shuangshuang Tan, Qinyou An,* and Liqiang Mai**

Rechargeable magnesium batteries (RMBs) have emerged as a promising candidate for next-generation energy storage due to their intrinsic safety and abundant resource availability. However, the development of ideal electrolytes that enable reversible Mg plating/stripping and ensure electrode compatibility remains a significant bottleneck. Over the past decades, considerable efforts have been devoted to addressing this challenge, highlighting the need for a comprehensive and fundamental understanding of the complex nature of Mg electrolytes. This review presents a comprehensive overview of the advances in nonaqueous Mg electrolytes, with an emphasis on solvation chemistry that governs ion transport, redox kinetics, and solid-electrolyte interphase formation. A systematic analysis of the interactions between ions and solvent molecules, namely active cations, anion receptors, weakly coordinated anions, and solvation structure, is offered to establish a fundamental understanding of structure-function relationships in Mg electrolytes. Furthermore, the key challenges and emerging research trends in Mg electrolytes are summarized. This work underscores the critical role of mastering solvation chemistry in optimizing RMB performance and provides principled guidance for rational, bottom-up Mg electrolyte design.

1. Introduction

Lithium-ion batteries (LIBs) have become integral to powering mobile devices such as smartphones, laptops, and electric vehicles since their commercialization in 1991.[1–3] However, safety concerns related to thermal runaway and the high cost of LIBs have restricted their suitability for large-scale energy storage applications.[4] To facilitate the decarbonization of the electrical grid, the development of high-energy and inherently safe, energy storage technologies is an increasingly pressing issue. Over the past few decades, emerging battery systems, including aqueous batteries, lithium metal batteries, and solid-state batteries, have been developed as next-generation alternatives for energy storage.[5–10] However, the narrow electrochemical window (≈1.23 V) of aqueous electrolytes limits their energy density, while dendrite formation in lithium metal batteries and solid-state batteries poses significant safety risks.[11–13] Uniform electrodeposition in high-capacity metal anodes is a fundamental requirement for battery systems to simultaneously achieve high energy density and robust operational safety. Among various candidate metal anodes, Mg metal stands out due to its dendrite-free plating morphology, which has been widely reported.[14,15] In addition, Mg metal features a high theoretical volumetric capacity (3833 mAh cm^{-3}), a low redox potential (−2.37 V vs standard hydrogen electrode), and abundant availability (≈2% in the earth's crust), making nonaqueous rechargeable magnesium batteries (RMBs) a highly promising energy storage technology.[14,16–20]

Since the prototype RMB was proposed in 2000, significant progress has been made in Mg electrolyte research.[21–26] However, the diversity and complex compositional complexity of Mg electrolytes continue to present challenges. To date, no standard RMB electrolyte has been established for either commercial or laboratory use. Most current studies categorize Mg electrolytes primarily based on salt and solvent species, which constrains a deeper understanding of the underlying interactions within electrolyte compositions.[27–29] In this review, we present a comprehensive analysis of solvation chemistry in nonaqueous Mg electrolytes, emphasizing the design of active cations, anion receptors, weakly coordinated anions, and solvation structures these four parts (**Figure 1**). By classifying electrolytes according to their intermolecular interaction mechanisms, this work seeks to deepen the understanding of the relationship between electrolyte microstructure and function. In addition, this review outlines key

J. Long, G. Zhang, Y. Ding, J. Zhang, P. Liu, H. Xu, Q. An, L. Mai
State Key Laboratory of Advanced Technology for Materials Synthesis and Processing
Wuhan University of Technology
Wuhan 430070, P. R. China
E-mail: anqinyou86@whut.edu.cn; mlq518@whut.edu.cn
S. Tan
College of Materials Science and Engineering
Chongqing University
Chongqing 400044, P. R. China
E-mail: tss@cqu.edu.cn
Z. He, R. Wang
Institute for Manufacturing
Department of Engineering
University of Cambridge
Cambridge CB3 0FS, UK
The ORCID identification number(s) for the author(s) of this article can be found under https://doi.org/10.1002/adma.202510488

DOI: 10.1002/adma.202510488

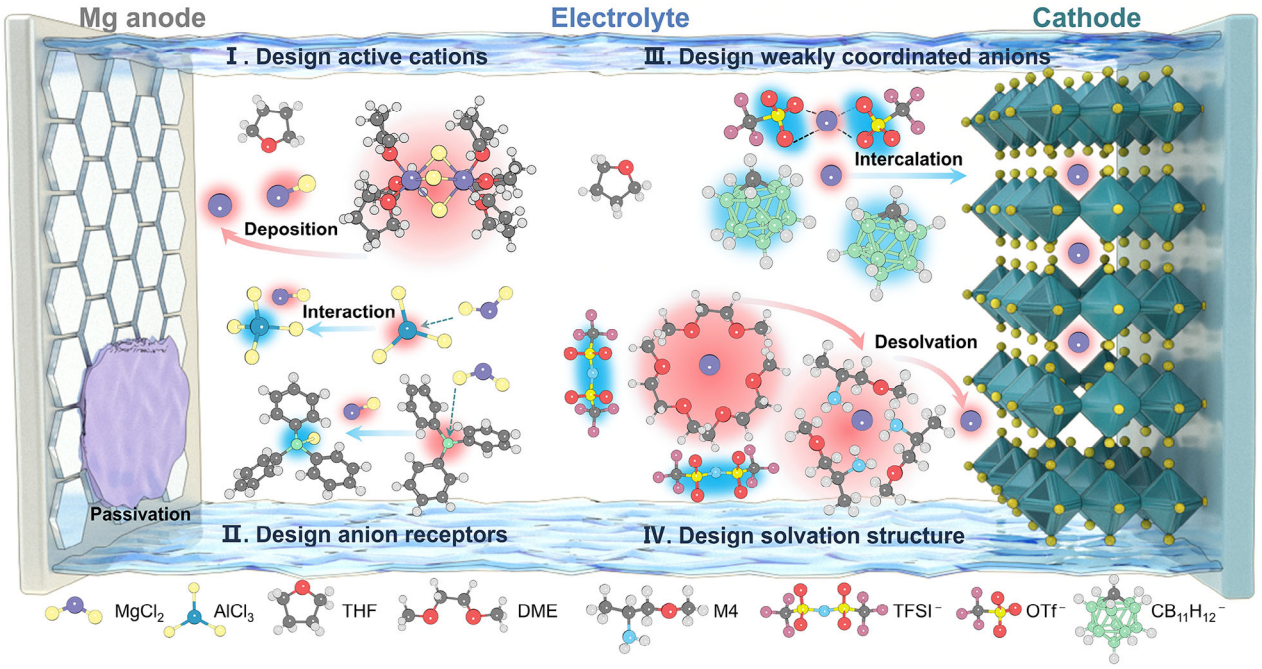

Figure 1. The schematic summarization of solvation chemistry in rechargeable magnesium batteries.

challenges and prospective directions in the development of Mg electrolytes, with considerations spanning both fundamental scientific issues and practical industrial needs. The established connection between solvation chemistry and electrolyte performance in RMBs not only provides valuable guidance for designing next-generation Mg electrolytes but also offers critical insights for advancing other multivalent ion batteries.

2. The Role of Solvation Chemistry in Mg Electrolytes

Solvation chemistry in electrolytes examines the interactions between solvent molecules and solutes (such as salts or additives) and their impact on electrode materials.[30] These interactions are typically stronger than those in gases but weaker than those in solids. While gaseous interactions can be analyzed using kinetic theory and solid-state interactions can be studied through solid-state physics, solution chemistry remains one of the most intricate area of physical chemistry.[31] Specifically, these intermolecular interactions in electrolytes include ion-ion, ion-solvent, and solvent-solvent interactions.

1) Ion-ion interactions are primarily governed by the Coulomb force, involving electrostatic attraction between oppositely charged ions and electrostatic repulsion between ions of the same charge. In the classical electrolyte model, the Coulomb force (F) is described by the following equation:

$$F = k\frac{q_1 q_2}{\varepsilon r^2}, k = 9.0 \times 10^9 N \cdot m^2/C^2 \quad (1)$$

where k represents the Coulomb constant, q_1 and q_2 are the charges of the two ions, ε is the dielectric constant of the solvent, and r is the distance between the ions. Factors such as ion charge, ion radius, ion configuration and electrolyte concentration all contribute to the strength of the Coulomb interaction. It is worth noting that the dielectric constant (ε) of organic solvent is significantly lower than that of water (80.2 at 20 °C)[31] which leads to a stronger Coulomb force in nonaqueous Mg electrolytes. The enhanced ion-ion interactions in electrolytes promote the formation of ion pairs (e.g., $MgCl^+$), ion clusters (e.g., $Mg_2Cl_3^+$),[32] and complexes (e.g., $[Mg_2(\mu\text{-}Cl)_3(THF)_6]^+$),[33] which subsequently influence salt solubility, electrolyte ionic conductivity, and the compatibility of electrode-electrolyte interphase.

2) Ion-solvent interactions arise from the solvation processes of cations and anions. These interactions are mainly driven by ion-dipole interactions and Lewis acid–base interactions. Typically, when a cation is coordinated with solvent molecules, it serves as an electron-pair acceptor, capturing electron pairs from the surrounding solvent molecules. The cation solvation structure determines the cation diffusion, de-solvation, and nucleation processes. Additionally, solvent molecules within the cation solvation shell are more readily able to accept electrons during reduction reactions compared to free solvent molecules in the bulk electrolyte, which accelerates solvent reductive decomposition. In contrast, these coordinated solvent molecules exhibit improved oxidative stability, as they are less prone to lossing electrons during oxidation reactions. Conversely, anion solvation enhances the reduction stability of the coordinated solvent while reduces its oxidation stability. However, due to their lower charge density compared to cations, the influence of anion solvation is less pronounced.[34] According to Frontier molecular orbital theory, these differences are reflected in lowered lowest unoccupied molecular orbital (LUMO) and highest occupied molecular orbital

(HOMO) energy levels for cation-coordinated solvents, while anion-coordinated solvents have higher LUMO/HOMO energy levels.[35] Typically, the ion-solvent interactions in a specified electrolyte can be fine-tuned by altering the coordinated anions or solvent molecules. This manipulation allows for controlled decomposition of selected components, resulting in the formation of an optimized solid electrolyte interphase (SEI) and cathode electrolyte interphase (CEI).[36–38]

3) Solvent-solvent interactions are primarily influenced by dipole-dipole interactions, hydrogen bonds, and Van der Waals forces. Dipole-dipole interactions arise exclusively in polar solvents, where the charge distribution imbalance within a molecule creates a dipole moment. In this situation, the positive charge center (δ^+) and the negative charge center (δ^-) of neighboring solvent molecules attract each other. Hydrogen bonds typically form between a partially positively charged H (covalently bonded to an electronegative atom or group) and another electronegative atom with a lone pair of electrons.[39] Hydrogen bonding is common in water and in organic compounds such as alcohols and ketones. Van der Waals forces, which exist between all molecules (polar and nonpolar), are weaker than the aforementioned two forces. Overall, solvent-solvent interactions play a key role in determining the solubility, freezing and boiling points, dielectric constant, vapor pressure, and viscosity of bulk electrolytes.

In practical electrolytes, solvation chemistry encompasses additional complex interactions, including dipole-induced dipole forces, instantaneous dipole-induced dipole forces, and hydrogen bonding between ions and solvent molecules. Nevertheless, ion-ion, ion-dipole, dipole-dipole interactions play a dominant role, which can be quantitatively described by the following equations:[31]

$$U_{\text{ion-ion}} = -\frac{1}{4\pi\varepsilon}\frac{z_1 z_2 e^2}{r} \quad (2)$$

$$U_{\text{ion-dipole}} = -\frac{1}{4\pi\varepsilon}\frac{ze\mu\cos\theta}{r^2} \quad (3)$$

$$U_{\text{dipole-dipole}} = -\frac{1}{(4\pi\varepsilon)^2}\frac{2{\mu_1}^2{\mu_2}^2}{3k_B T_r^6} \quad (4)$$

In addition to the charge of ion (ze) and the angle between the dipole moment (μ) and the line connecting the ion and the center of the dipole (θ), the dielectric constant (ε) of solvent and the interaction distance (r) between ions and dipoles determine the strength of these forces.[40] Specifically, changes in the dielectric constant or the anion radius can regulate the solvation effect, influencing the binding energies of ion-ion and ion-solvent interactions. These changes, in turn, affect the ions' solvation structures, the electrolytes' electrochemical stability windows, and the electrode-electrolyte interphase properties (**Figure 2**).

3. The Key Challenges in Mg Electrolytes and the Resolution Strategies

Solvation chemistry in electrolytes is driven by the dissociation of the crystalline salt and the subsequent solvation of ions. Both

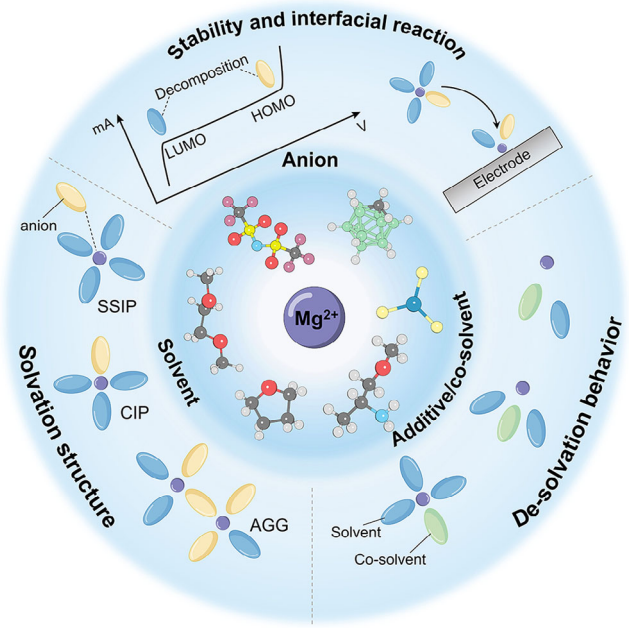

Figure 2. Illustration of the interaction types in Mg electrolytes and their relationships with solvation structure, de-solvation process, electrochemical stability, and interfacial reaction.

a lower lattice energy (typically represented by the salt's melting point) and a higher solvation energy favor salt dissolution.[40,41] Mg salts generally possess a higher melting point than Li salts (714 °C of $MgCl_2$ vs 605 °C of LiCl). Additionally, the smaller cation radius (0.72 Å of Mg^{2+} vs 0.76 Å of Li^+) and the divalent nature of Mg^{2+} result in stronger ion-ion ($U_{ion\text{-}ion}$) and ion-solvent ($U_{ion\text{-}dipole}$) interactions. Furthermore, the stronger Lewis acidity of Mg^{2+} compared to Li^+ leads to stronger Lewis acid-base interactions with the solvent molecules, which results in a significantly larger Stokes radius for Mg^{2+} than Li^+ (3.47 Å vs 2.38 Å in water).[42,43] Consequently, Mg^{2+} forms more robust coordination with both anions and solvent molecules. These strong interactions promote the formation of tightly bonded contact ion pairs (CIPs), aggregates (AGGs), or solvent-separated ion pairs (SSIPs) structures in Mg electrolytes,[44] thereby hindering the "free-flowing" state of Mg^{2+} in solution. Moreover, the currently used Mg electrolytes are primarily based on ether solvents, which offer high interphase compatibility but exhibit a lower dielectric constant compared to other solvents (**Table 1**). Thus, both the solubility of Mg salts and electrolytes' ionic conductivity are considerably lower than those in Li-based systems.

I. To reduce ion-ion interactions and ensure the complete dissociation of Mg salts in ether-based solvents, charge-delocalized anions with strong electron-withdrawing groups are employed (such as $TFSI^-$, OTf^-, ClO_4^-).[45,46] However, due to the strong electron-accepting nature of divalent Mg^{2+}, coordinated solvents and anions typically exhibit much lower LUMO energy levels, making them more likely to decompose and ultimately passivate the Mg metal anode.[47] Therefore, designing electroactive cations or cation clusters

Table 1. Physical properties of the common organic solvents for RMB electrolytes.

Solvent	Chemical structure	Coordinating sites	T_m [°C]	T_b [°C]	η [cP] [25 °C]	Density [g mL^{-1}]	ε	DN
THF		sp^3O (ether)	−108	66	0.55	0.887	7.1	20
DOL		sp^3O (ether)	−95	75	0.53	1.06	7.1	18
DME	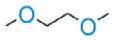	sp^3O (ether)	−58	84	0.46	0.867	7.2	20
G2	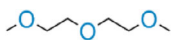	sp^3O (ether)	−60	162	1.06	0.944	7.4	19.5
G3	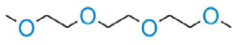	sp^3O (ether)	−45	216	2.18	0.986	7.6	14
G4	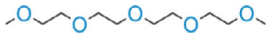	sp^3O (ether)	−30	275	3.39	1.009	7.7	16.6
BTFE	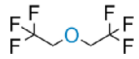	sp^3O (ether)	25	62	0.64	1.414	13.4	<10
MOEA	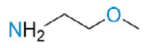	sp^3O (ether)/ sp^3N (amine)	−82	95	0.66	0.864	9	64.8
DMA		sp^2O (carbonate)/ sp^3N (amine)	<20	184	0.92	0.925	36.7	27.8
TMP		sp^2O (carbonate)	−46	197	2.032	1.197	20.6	23
TEP	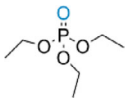	sp^2O (carbonate)	−56	215	1.7	1.072	13.1	23.4
EC		sp^2O (carbonate)	36	248	1.9 (40 °C)	1.321	89.7	16.4
PC		sp^2O (carbonate)	−48	242	2.53	1.204	64.9	15.1
NMI		sp^2N (imidazole)	−60	198	1.382 (35 °C)	1.03	39	47
ACN	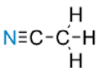	sp N	−45	82	0.38	0.786	37.5	14.1
DMSO	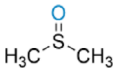	sp^2O (sulfoxide)	18.4	189	1.99	1.1	46.7	30
H_2O		sp^3O (hydroxyl)	0	100	0.899	1	80.2	18

is one of the most effective ways to achieve reversible Mg plating/stripping.

II. On the other hand, some commercially available Mg salts (such as $MgCl_2$) demonstrate high Mg anode affinity but have limited solubility in ether solvents.[48,49] Strengthening anion-dipole interactions can improve the solubility of these Mg salts. The introduction of strong anion acceptors facilitates electron pair acceptance from anions via Lewis acid-base interactions. The resulting coordinated-anions structure not only promotes Mg salt dissociation but also expands the electrolyte's electrochemical stability window.[50] Accordingly, designing a variety of multifunctional anion receptors is another optimization strategy for Mg electrolytes.

III. Designing weakly coordinated anions is a further approach to minimizing ion-ion interactions in Mg electrolytes. Reducing the strong Mg^{2+}-anion electrostatic interaction requires a larger anion radius and more electron-withdrawing groups. The large ionic radius of anions enables a more uniform dispersion of negative charges, which weakly coordinate with Mg^{2+}, thereby increasing the solubility of Mg salts. Furthermore, the presence of electron-withdrawing groups

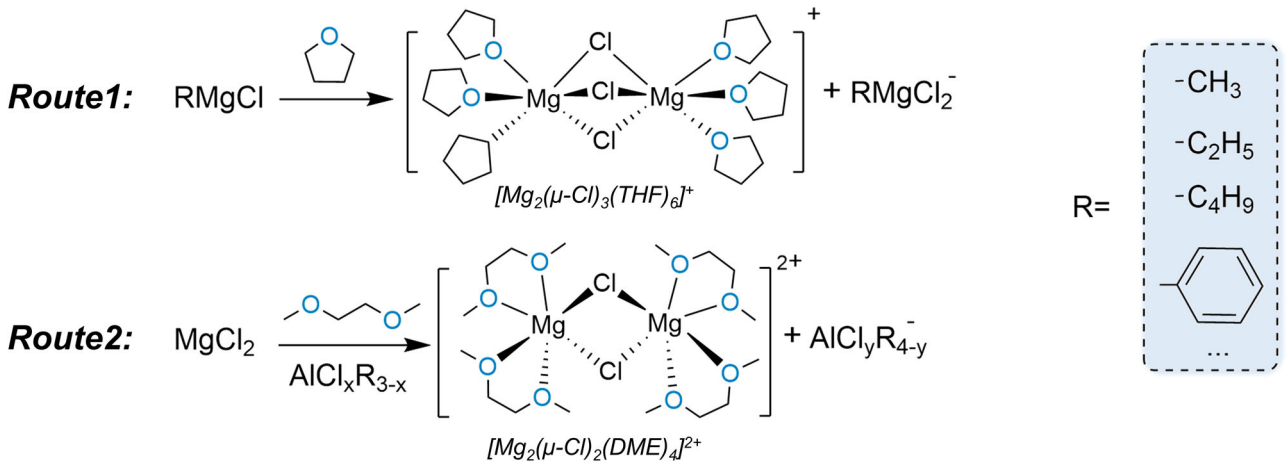

Scheme 1. Typical reaction routes and structural illustration of $[Mg_2(\mu\text{-}Cl)_3(THF)_6]^+$ and $[Mg_2(\mu\text{-}Cl)_2(DME)_4]^{2+}$ cations.

can reduce the HOMO energy level of the anion, enhancing the oxidation stability of the electrolyte.[51]

IV. Regulate ion-ion and ion-dipole interactions to optimize Mg^{2+} solvation structure and enable reversible Mg plating/stripping. The electrolyte solvation structure plays a critical role in determining ion diffusion rates, the desolvation process, and electrode-electrolyte interphase behavior. The primary solvation sheath is formed by the competitive coordination between Mg^{2+} and electron donors, such as solvents and anions. By introducing tailored components into the solvation structure, the strength of the Mg^{2+}-electron donor interaction can be regulated, facilitating rapid Mg^{2+} diffusion and promoting the formation of a stable, passivation-free Mg anode interphase.[52] In summary, a comprehensive understanding of solvation chemistry is vital for the rational design of high-performance Mg electrolytes. In the subsequent sections, we will delve deeper into the four key aspects outlined above, providing a detailed analysis of their implications for electrolyte performance.

4. Strategies for Regulating the Solvation Chemistry in RMBs

4.1. Design Active Cations

As early as 1957, reversible Mg plating/stripping has been demonstrated in ether solutions of C_2H_5MgBr or $MgBr_2$, although the plating efficiency was relatively low (≈71%).[49] Modifying the alkyl group (R) of the Grignard reagent RMgX (X = Cl or Br) can further enhance Coulombic efficiency (CE). In these solutions, the Mg^{2+} diffusion and reduction mechanisms differ significantly from those in Li-based batteries, where Li^+ migrates through a stable SEI film and subsequently undergoes reduction. In contrast, the reversible Mg redox in Grignard reagent involves a complex electrolyte component adsorption-desorption process, rather than a simple two-electron transfer reaction.[53,54] This distinct reduction pathway prevents the passivation of Mg metal in such systems. The possible equilibria are established in these solutions:

$$2RMgX \leftrightarrow MgR_2 + MgX_2 \text{ Schleck equilibrium} \quad (5)$$

$$2RMgX \leftrightarrow RMg^+ + RMgX_2^- \text{ Ionization equilibrium} \quad (6)$$

Scheme 1 summarizes the two most common active cations derived from ionization equilibrium. Specifically, the major active cations in Grignard reagents was investigated by Sakamoto et al. using single-crystal X-ray diffraction (XRD).[55] They found that active $[Mg_2(\mu\text{-}Cl)_3(THF)_6]^+$ cation or $R_2Mg_4Cl_6(THF)_6$ structure is prevalent in various Grignard reagents (with R groups such as Me, Bu, Ph, or benzyl), which are responsible for highly reversible Mg plating/stripping (**Figure 3**a,b). However, as strong reducing agents, Grignard reagents suffer from insufficient oxidation stability, making them difficult to match with cathodes and therefore unsuitable for practical Mg batteries. To solve this problem, Aurbach et al. introduced a family of Mg organohaloaluminate salts ($Mg(AlCl_3R)_2$ and $Mg(AlCl_2RR')_2$). When dissolved in tetrahydrofuran (THF), Mg salts with alkyl groups (Et and Bu) exhibit nearly 100% Mg plating/stripping efficiency. Additionally, the wide electrochemical window of these electrolytes enables compatibility with Chevrel phase Mo_6S_8 cathode, as assembled RMB prototype systems delivered steady cycling for over 2000 cycles.[21] Their further investigations revealed that the active $[Mg_2(\mu\text{-}Cl)_3(THF)_6]^+$ cation is still commonly found in these electrolytes (Figure 3c).[56] Consequently, $[Mg_2(\mu\text{-}Cl)_3(THF)_6]^+$ has been widely recognized as the most effective active cation for facilitating reversible Mg redox reactions.

To investigate the anti-passivation mechanism of the active $[Mg_2(\mu\text{-}Cl)_3(THF)_6]^+$ cation during the Mg deposition, Kim et al. identified three potential Mg-deposition pathways through ab initio calculations, all of which involve a multi-step reduction mechanism.[54] Similarly, Benmayza et al. proposed a three-step reduction mechanism based on in situ X-ray absorption measurements, which involves the dissociation of the $[Mg_2(\mu\text{-}Cl)_3(THF)_6]^+$ dimer, the adsorption of $[MgCl(THF)_5]^+$ monomers onto the Mg anode, and the subsequent electroreduction of Mg^{2+} to Mg^0.[32] Overall, in contrast to the direct two-electron

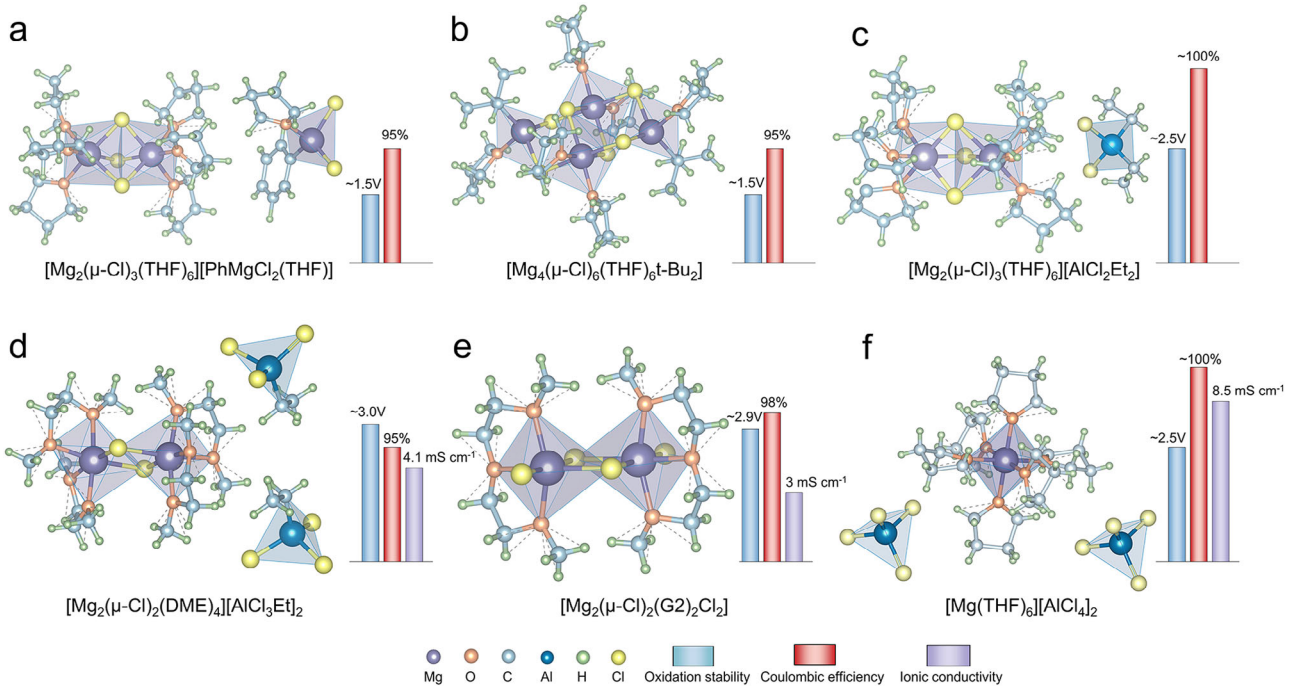

Figure 3. Single crystal structure and electrochemical properties of a) $[Mg_2(\mu\text{-}Cl)_3(THF)_6][PhMgCl_2(THF)]$, b) $[Mg_4(\mu\text{-}Cl)_6(THF)_6t\text{-}Bu_2]$, c) $[Mg_2(\mu\text{-}Cl)_3(THF)_6][AlCl_2Et_2]$, d) $[Mg_2(\mu\text{-}Cl)_2(DME)_4][AlCl_3Et]_2$, e) $[Mg_2(\mu\text{-}Cl)_2(G2)_2Cl_2]$, and f) $[Mg(THF)_6][AlCl_4]_2$.

reduction of Mg^{2+}, the unique adsorption-reduction mechanism of $[Mg_2(\mu\text{-}Cl)_3(THF)_6]^+$ cations, effectively prevents the passivation of the Mg anode, which is critical for reversible Mg plating/stripping.[57] However, the bulky coordination structure of $[Mg_2(\mu\text{-}Cl)_3(THF)_6]^+$ hampers both the diffusion coefficient of Mg^{2+} and the ionic conductivity of the electrolyte. Therefore, the development of more flexible and kinetically favorable active cations is essential to overcome these limitations.

Although THF demonstrates excellent compatibility with the Mg metal anode, its high volatility restricts its practical applications. Among various ether solvents, DME stands out for its superior thermal and chemical stability, making it a preferred choice in Li-ion and Na-ion batteries.[30,58] Additionally, compared to the single coordination oxygen in a THF molecule, the DME chain contains two coordination oxygens, which can reduce the number of coordinated solvents and promote a more flexible active cation structure. Cheng et al. first identified the active Mg cation structure in DME-based Mg electrolytes. Their crystallographic analysis revealed that the electroactive complex $[Mg_2(\mu\text{-}Cl)_2(DME)_4]^{2+}$ is commonly observed across a range of DME-based electrolytes (Figure 3d).[59] Besides, these electrolytes demonstrated the lowest Mg plating overpotential (≈220 mV), the higher CEs (≈95%), and ionic conductivity (≈4.1 mS cm^{-1}) among various ether-based electrolytes, such as THF, G2, G3, or G4. Further optimization of the electrolyte performance can be achieved by increasing the concentration of the thermodynamically stable $[Mg_2(\mu\text{-}Cl)_2(DME)_4]^{2+}$ cation. The optimized electrolyte exhibits a decent electrochemical window of 3.5 V and excellent compatibility with the Mo_6S_8 cathode.

In general, electroactive $Mg_xCl_y^+$ cation clusters are commonly found in chlorine-containing Mg electrolytes (Figure 3e), which are responsible for a passivation-free Mg plating/stripping process.[60,61] However, these Mg-Cl coordinated structure leads to increased corrosion and decreased Mg^{2+} conductivity in the electrolyte.

To address this problem, Zhang et al. developed an electroactive $[Mg(THF)_6][AlCl_4]_2$ salt through a simple heating process in an ionic liquid (Figure 3f). The mono-Mg^{2+} as active cations reduces the corrosiveness of the electrolyte, while the smaller $[Mg(THF)_6]^{2+}$ structure promotes faster Mg^{2+} diffusion. This non-nucleophilic electrolyte structure enables the reversible cycling of the Mg-S batteries for 20 cycles.[62] Moreover, they applied a similar thermal strategy in a DME-based electrolyte to synthesize a $[Mg(DME)_2][(HMDSAlCl_3)]_2$ complex. By incorporating hexamethyldisilazide (HMDS) groups in the anions, the electrolyte's corrosion rate was further reduced, its oxidation stability (≈3.5 V) was enhanced, and the cyclability of Mg-S batteries was extended to 100 cycles.[63]

Overall, early research on Mg electrolytes focused on halogen-containing electrolytes, as they enable reversible Mg redox reactions.[61,64] The existence of electroactive $Mg_xCl_y^+$ ion clusters can reduce the electrolyte activation process, while the adsorption of chlorine-containing components on the anode interphase can protect Mg metal from passivation.[64–67] As a result, these electrolytes have been extensively applied in various cathode materials, such as sulfides and selenides.[68,69] However, the low oxidation stability and limited concentration of these electrolytes restrict their practical application in high-voltage cathode systems, indicating a need for further improvement.[70]

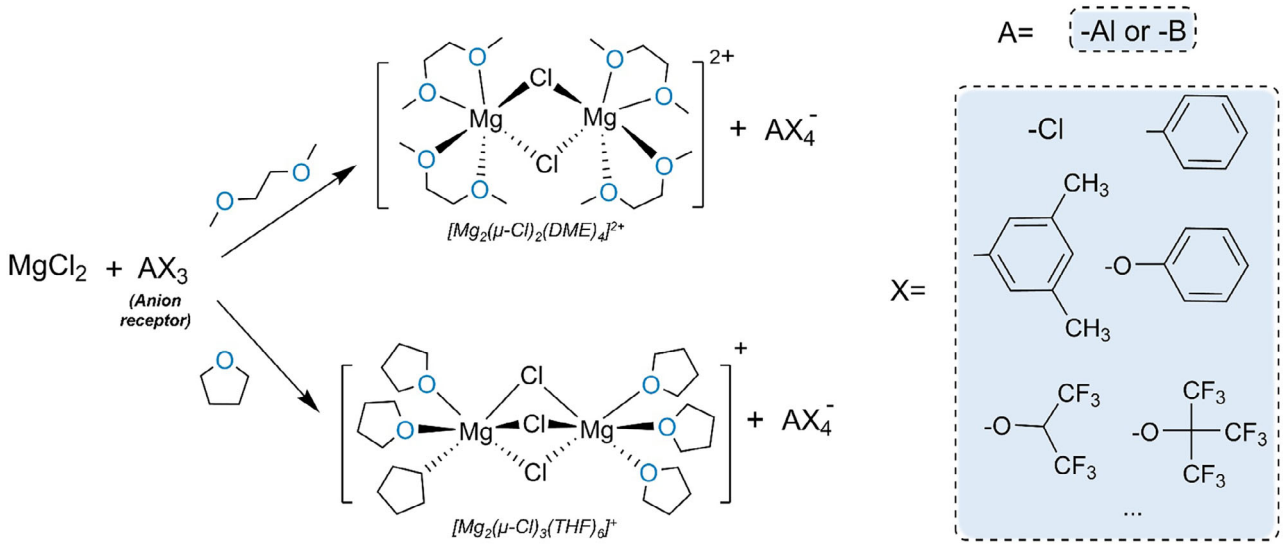

Scheme 2. Typical reaction routes between $MgCl_2$ and anion receptors in THF and DME solvents.

4.2. Design Anion Receptors

Electrolyte solvents with high dielectric constants can weaken cation-anion interactions and promote ionic dissociation, resulting in enhanced ionic conductivity and salt solubility. However, passivation-free Mg redox reactions have predominantly been observed in low dielectric constant solvents, such as ethers or amines.[71] Therefore, designing anion receptors to capture anions and release active Mg cations represents another important strategy (**Scheme 2**). Since anions are the more easily oxidized components in the solution, they largely determine the oxidation stability of the electrolyte. The interaction between anion receptors and anions will generate a bulky anion structure, facilitating electron delocalization and significantly improving the high-voltage stability of the electrolyte.

Among various reagents, $AlCl_3$ is the most widely used anion receptor (**Figure 4**). In its molecule structure, the central aluminum (Al) atom adopts sp^2 hybridization, forming three covalent bonds with three Cl atoms while retaining a vacant p-orbital capable of accepting an electron pair from anions. Additionally, due to the higher electronegativity of Cl atoms compared to the Al atom, the electron cloud density around the Al atom is reduced, imparting strong Lewis acidity to $AlCl_3$. This enhanced acidity enables $AlCl_3$ to effectively coordinate with anions possessing lone electron pairs through ligand bonding, forming stable complexes.

Aurbach et al. pioneered the combination of $AlCl_3$ with a Grignard reagent (PhMgCl) in THF, synthesizing the all-phenyl complex (APC) electrolyte through a transmetalation reaction.[72] Comprehensive analyses using Raman spectroscopy, NMR spectroscopy, single crystal XRD, and DFT calculation confirmed that the equilibrium species in the APC electrolyte are $AlCl_{(4-n)}Ph_n^-$ anions (**Figure 5a**). The APC electrolyte provides a electrochemical window of over 3 V and achieves nearly 100% Mg plating/stripping efficiency with low polarization (< 0.2 V).[73] The introduction of $AlCl_3$ promotes Mg^{2+} dissociation, resulting in an ionic conductivity for the APC electrolyte comparable to that of standard Li-ion battery electrolytes within the temperature range of −10 to 30 °C (≈4 mS cm^{-1}). This work paves the way for designing anion receptors to improve electrolyte performance. Despite the significant advancements of APC electrolytes in various aspects, their commercial application remains limited due to the use of air- and water-sensitive organometallic Grignard reagents. Doe et al. developed the first fully inorganic Magnesium Aluminum Chloride Complex (MACC) electrolyte through a Lewis acid-base reaction between $MgCl_2$ and $AlCl_3$. This electrolyte exhibits decent anodic stability (≈3.1 V), excellent Mg plating/stripping efficiency (99%), and low overpotential (<0.2 V) (Figure 5b). More importantly, the use of cost-effective $MgCl_2$ salts as the Mg source makes this electrolyte more commercially viable.[74]

By reacting $AlCl_3$ with Mg salts containing varied functional groups, electrolytes with precisely tailored properties can be prepared. The performance of the non-nucleophilic hexamethyldisilazide magnesium chloride (HMDSMgCl) electrolyte can be enhanced by the addition of $AlCl_3$.[75,76] The prepared HMDSMgCl-$AlCl_3$ electrolyte exhibited good compatibility with the electrophilic sulfur cathode. Moreover, the purified $[Mg_2(\mu\text{-}Cl)_3(THF)_6][HMDSAlCl_3]$ crystalline electrolyte (Figure 5c), showed significant improvements in both oxidation stability (≈3.2 V) and plating/stripping efficiency (≈100%). As a proof of concept, the first assembled Mg-S battery achieved an impressive initial capacity of 1200 mAh g^{-1}. Despite rapid capacity decay was observed due to the polysulfide "shuttle effect", this work represents a significant step toward advancing Mg-S batteries. Fichtner et al. further simplified the synthesis of HMDS-based electrolytes.[77] They replaced HMDSMgCl with $Mg(HMDS)_2$ and $MgCl_2$ to react with $AlCl_3$. The addition of $MgCl_2$ in the electrolyte drives the ionization equilibrium as follows:

$$HMDSAlCl_2 + 2MgCl_2 \leftrightarrow [Mg_2Cl_3][HMDSAlCl_3] \quad (7)$$

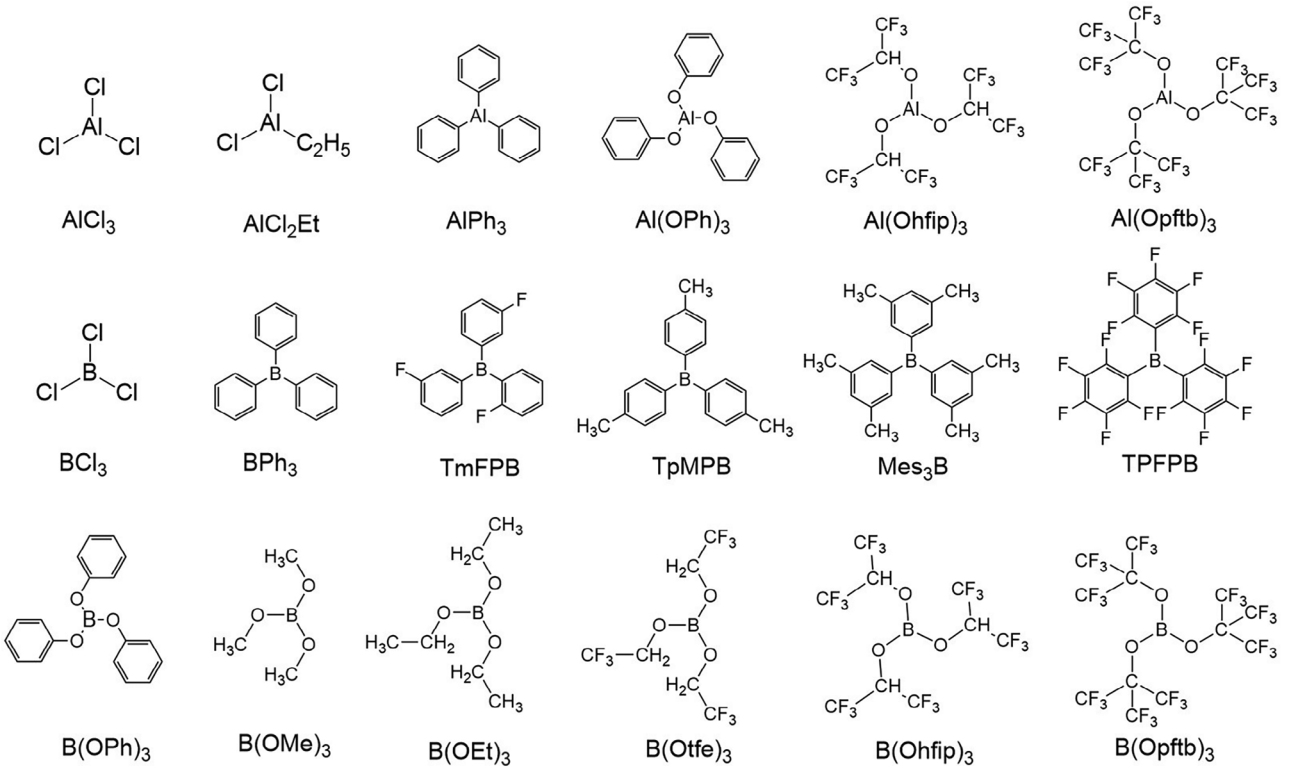

Figure 4. Commonly used Aluminum/Boron-based anions receptors in RMB electrolytes.

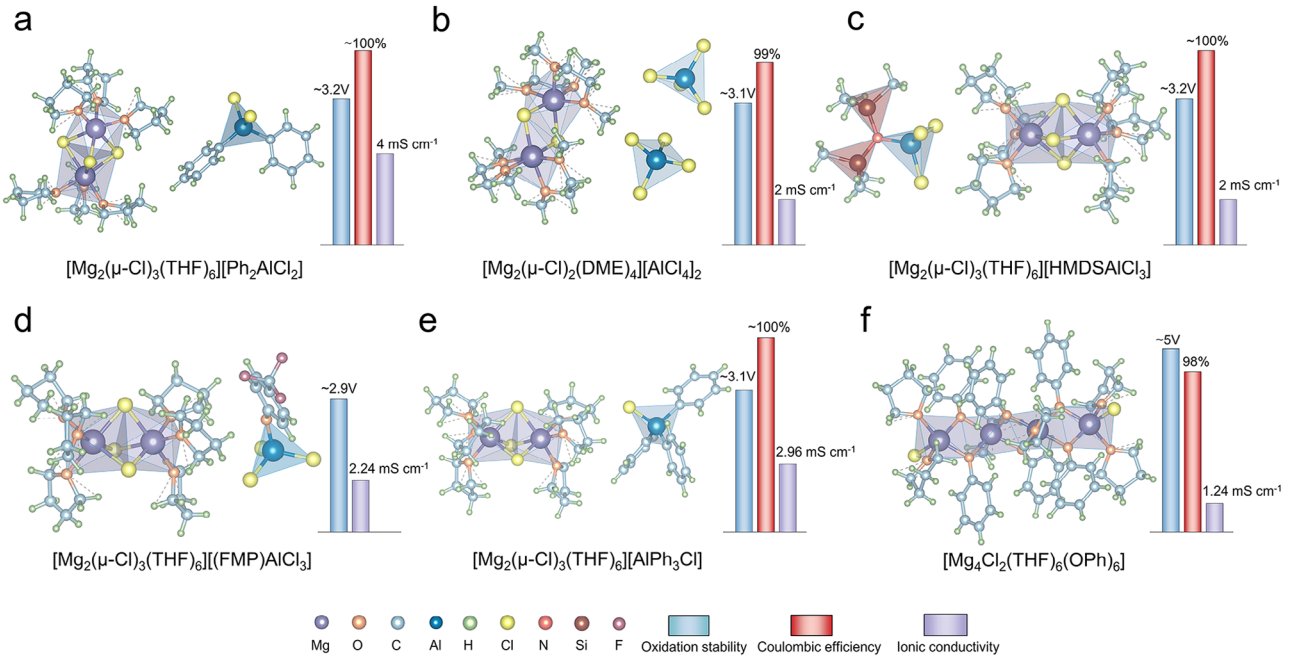

Figure 5. Single crystal structure and electrochemical properties of a) $[Mg_2(\mu\text{-}Cl)_3(THF)_6][Ph_2AlCl_2]$, b) $[Mg_2(\mu\text{-}Cl)_2(DME)_4][AlCl_4]_2$, c) $[Mg_2(\mu\text{-}Cl)_3(THF)_6][HMDSAlCl_3]$, d) $[Mg_2(\mu\text{-}Cl)_3(THF)_6][(FMP)AlCl_3]$, e) $[Mg_2(\mu\text{-}Cl)_3(THF)_6][AlPh_3Cl]$, and f) $[Mg_4Cl_2(THF)_6(OPh)_6]$.

This reaction results in a high concentration of electroactive $[Mg_2Cl_3][HMDSAlCl_3]$ species, granting the electrolyte high oxidation stability (>3.5 V). By increasing the Mg^{2+} concentration to 1.8 M and introducing an ionic liquid co-solvent, they mitigated Mg polysulfide dissolution and the shuttle effect. Based on this modified electrolyte, the assembled Mg-S batteries achieve a high discharge plateau of 1.65 V, which is close to the theoretical thermodynamic value. In addition to synthesizing non-nucleophilic electrolyte, $AlCl_3$ can improve the oxidative stability of electrolytes when combined with Mg salts containing electron-withdrawing groups.[78] Similarly, $AlCl_3$ complexation with phenolate-based Mg salts enhances the electrolyte's resistance to moisture and oxygen (Figure 5d).[79,80] In summary, the incorporation of diverse functional groups into the electrolyte enables the design of multifunctional Mg electrolytes.[81–83]

Inspired by the great success of $AlCl_3$, several analogous Al-centered anion receptors have also attracted significant attention.[84,85] Liu et al. reported the combination of $MgCl_2$ with various Al-centered anion receptors ($AlCl_3$, $AlCl_2Et$, and $AlPh_3$). Their findings revealed that these electrolytes share the same $[Mg_2(\mu\text{-}Cl)_3(THF)_6]^+$ active cation (Figure 5e), demonstrating moderate oxidation stability (≈3 V) and high electrochemical reversibility (≈100% CEs).[86] Bartlett et al. designed a phenolate-based $Al(OPh)_3$ anion receptor.[87] When complexed with PhMgCl at a 1:4 ratio, it produces a low-chlorine-content electrolyte with unprecedented oxidative stability (Figure 5f), exceeding 5 V on both stainless steel (SS) and platinum (Pt) current collectors—the highest oxidative stability reported for Mg electrolytes so far. Unfortunately, this electrolyte shows poor cathode compatibility, and its detailed anti-oxidation anion structure remains unclear. Nevertheless, the expanded electrochemical window of this electrolyte presents a promising pathway for the development of high-voltage RMBs.

Overall, Al-centered anion receptors play a crucial role in promoting Mg salt dissociation and improving both the oxidation stability and reversibility of electrolytes. However, the Al/Al^{3+} redox couple possesses a higher redox potential (−1.66 V vs SHE) compared to the Mg/Mg^{2+} couple (−2.37 V vs SHE), the formed $AlCl_2^+$ cation would lead to irreversible Al deposition during Mg^{2+} reduction. This phenomenon reduces Coulombic efficiency and necessitates a "conditioning" process to optimize electrolyte performance.[64,88–90] Consequently, researchers have shifted their focus toward developing boron (B)-centered anion receptors as alternatives to Al-centered systems.

B and Al, both belonging to the same main group with three valence electrons, adopt *sp2* hybridization and retain an empty orbital when forming compounds, enabling them to function as anion acceptors. Due to its smaller atomic radius compared to Al, B exhibits stronger electron attraction and non-metallic behavior, which does not deposit during Mg reduction. Additionally, B's higher electronegativity (2.04) compared to Al (1.61) gives B-based anion receptors stronger Lewis acidity, making them more effective at binding anions and forming stable structures. Furthermore, B and its compounds are highly compatible with various electrode materials.[91] These advantages make B-centered anion receptors highly attractive alternatives to Al-centered anion receptors. In lithium-ion batteries, boron-based additives have been reported to promote the formation of a protective cathode electrolyte interphase (CEI) and mitigate cathode material dissolution and structural degradation during cycling, leading to enhanced battery performance.[92]

Early B-centered anion receptors can be traced back to BCl_3 and BPh_3. However, the prepared BPh_3-based electrolytes exhibited lower Coulombic efficiency and reduced decomposition potential compared to their Al-centered counterparts (**Figure 6a**).[24,56] In 2012, Guo et al. functionalized the benzene ring of BPh_3 with methyl or fluoro groups via a modified organometallic reaction.[50,93] The resulting triarylborates BR_3-PhMgCl electrolytes exhibited efficient Mg plating/stripping abilities. Notably, dimethyl-substituted aryl borates (Mes_3B, Mes = 3,5-$Me_2C_6H_3$)-PhMgCl electrolyte displayed superior cathode compatibility and the highest oxidation stability (≈3.5 V) (Figure 6b). Their analysis revealed that the enhanced stability arises from an intermediate product formed via weak interactions between the $[Mes_3BPh]^-$ anion and Ph_2Mg. However, the presence of chlorine compromises the high oxidation stability of this electrolyte, confining its applicability to corrosion-resistant Pt electrodes. To enhance the practical applicability of Mes_3B, they substituted the Grignard reagent PhMgCl with chlorine-free $MgPh_2$ salts as the Mg source. The resulting $Mg[Mes_3BPh]_2$/THF electrolyte demonstrated comparable oxidation stability (>2.5 V) on Pt, SS, and Al current collectors.[94]

In addition to methyl substitution, An et al. demonstrated that fluoro-substitution also introduces functional properties to aryl B-centered anion receptors.[95] They incorporated the fully fluorinated anion receptors tris(pentafluorophenyl)boron (TPFPB) into a $B(OPh)_3$-$MgCl_2$-THF electrolyte. The strong electron-withdrawing effect of the -F groups significantly increased the Lewis acidity of TPFPB. When combined with $MgCl_2$, more active $[Mg_2Cl_3]^+$ species were generated, improving the electrolyte's Mg plating/stripping reversibility. More importantly, the decomposition of this TPFPB additive facilitated the formation of an MgF_2-rich SEI layer, which suppressed side reactions and enhanced the long-term cycling performance of RMBs. In summary, tailoring functional groups on the benzene ring represents a promising and practical strategy for developing multifunctional anion receptors, offering significant potential for further exploration.

Fluorination of the terminal group also has a positive effect on alkyl B-centered anion receptors. Cui et al. designed a borate ester ($B(Ohfip)_3$) with trifluoromethyl (-CF_3) terminal groups. Compared with -F group, the strong electron-withdrawing effect of the -CF_3 groups endows the reagent with stronger Lewis acidity, facilitating the dissolution of various insoluble Mg salts, including MgO,[96] MgF_2,[97] $Mg(BH_4)_2$,[98] and $MgCl_2$.[99] Although the active cations in these electrolytes differ—namely, $[(DME)_2Mg\text{-}O\text{-}Mg]^{2+}$, $[Mg(DME)_n]^{2+}$, $[MgBH_4(DME)_2]^+$, and $[Mg_4Cl_6(DME)_6]^{2+}$—their anionic structure evolves into the same $[B(Ohfip)_4]^-$ anions during cycling (Figure 6c,d). This bulky, electron-delocalized anion structure shows lower HOMO energy level, broadening the electrolytes' electrochemical stability window. Its non-nucleophilic nature enables good compatibility with high-capacity S or Se cathodes. As a result, the Mg-Se batteries with BCM (MgF_2-$B(Ohfip)_3$) electrolyte maintain a capacity of 361 mAh g^{-1} after 200 cycles, and the Mg-S batteries with OMBB electrolyte (Mg-$MgCl_2$-$B(Ohfip)_3$) deliver an impressive capacity of 1019 mAh g^{-1} after 100 cycles. Recently, Jin et al. developed a simpler in situ reaction strategy involving $B(Ohfip)_3$,

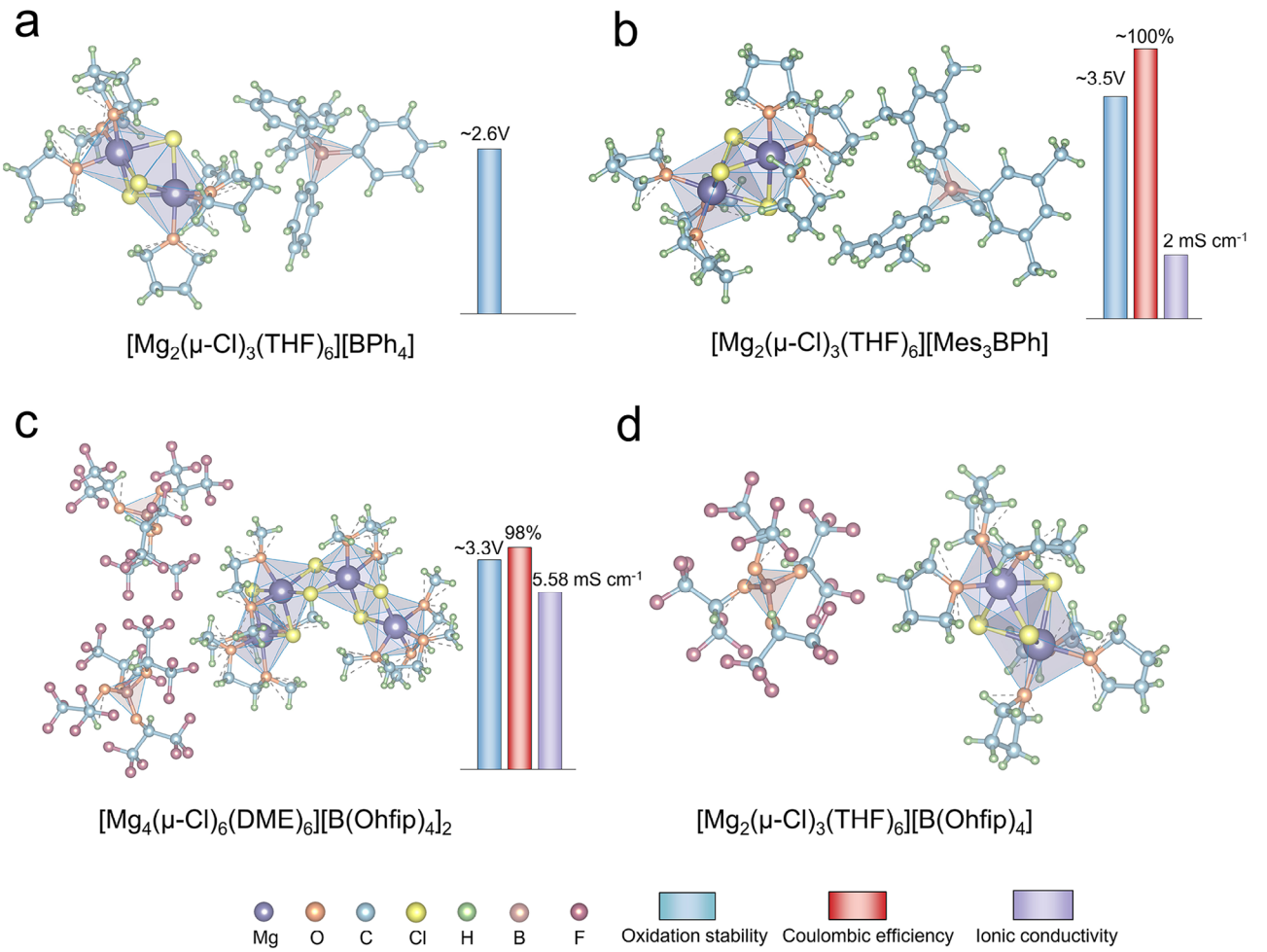

Figure 6. Single crystal structure and electrochemical properties of a) $[Mg_2(\mu\text{-}Cl)_3(THF)_6][BPh_4]$, b) $[Mg_2(\mu\text{-}Cl)_3(THF)_6][Mes_3BPh]$, c) $[Mg_4(\mu\text{-}Cl)_6(DME)_6][B(Ohfip)_4]_2$, and d) $[Mg_2(\mu\text{-}Cl)_3(THF)_6][B(Ohfip)_4]$.

I_2, and the Mg metal anode.[100] Unlike conventional Lewis acid-base reactions between $B(Ohfip)_3$ and Mg salts, this in situ interfacial reaction promotes the formation of an MgI_2- and MgF_2-rich SEI layer on the Mg anode. This favorable interphase extends the Mg anode's cycle life to 1500 h with a low overpotential of 80 mV. Beyond its application in chlorine-containing electrolytes, the strong anion-accepting ability of $B(Ohfip)_3$ allow for the construction of chlorine-free, weakly coordinated electrolyte system, which will be discussed in detail in the following section.

Building on the success of bis-trifluoromethyl substituted $B(Ohfip)_3$, mono-trifluoromethyl substituted $B(Otfe)_3$ anion receptors present a cost-effective alternative for B-based electrolytes.[101,102] Additionally, the reduced steric hindrance of $B(Otfe)_3$ enables more rapid and efficient interactions with Mg salts. Similar to $B(Ohfip)_3$-based electrolytes, when $B(Otfe)_3$ complexes with $MgCl_2$ or MgF_2 salts, both electrolytes feature the same $[B(Otfe)_4]^-$ anion structure, but differ in their cations: $[Mg_2Cl_2(THF)_6]^{2+}$ and $[Mg(DME)_3]^{2+}$, respectively. In these structure, the chlorine-free $[Mg(DME)_3]^{2+}$ cation has a significantly higher de-solvation energy barrier than $[Mg_2Cl_2(THF)_6]^{2+}$ cation, which may be responsible for its inferior Mg plating/stripping efficiency. Benefiting from the diverse structural configurations of B/Al-based anion receptors, the mono-trifluoromethyl substituted $Al(Otfe)_3$, tris-trifluoromethyl substituted $Al(Opftb)_3$, $B(Opftb)_3$, and other Al- or B-centered derivatives hold significant potential for advancing RMBs technology.

It is worth mentioning that reagents like $CrCl_3$ and $InCl_3$ possess molecular structures similar to $AlCl_3$, yet their roles in Mg batteries extends beyond serving as anion receptors. For instance, adding $CrCl_3$ to the MACC electrolyte results in the formation of nanoscale Cr-rich deposits, which act as heterogeneous catalysts. These deposits enable the selective deposition of Al and facilitate the rapid dissolution of Mg, thereby yielding a "conditioning-free" MACC electrolyte.[103,104] Additionally, the $Mg(OTf)_2$-$InCl_3$ complexed electrolyte promotes the in situ formation of a Mg–In alloy interphase. This Mg-philic interphase facilitates uniform Mg deposition and accelerates redox reaction kinetics.[105,106]

In addition to reagents with vacant coordination orbitals that function as anion receptors, some soluble metal salts can release cations that interact with insoluble Mg salts, enhancing their solubility and improving electrolyte performance. This mechanism represents another class of "anion receptors" (**Figure 7**), with Li salts being the most prevalent example. As we previously highlighted, Li salts exhibit superior solubility relative to Mg salts

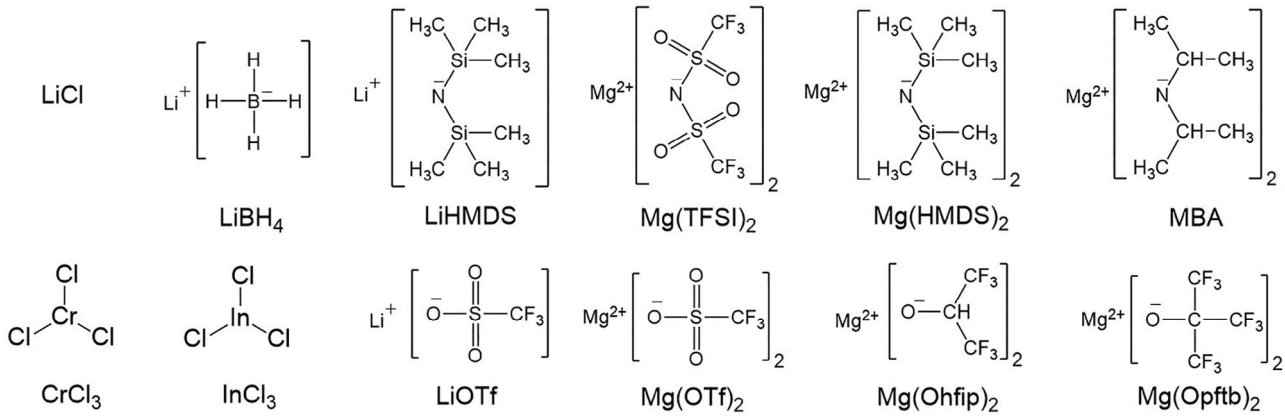

Figure 7. Commonly used co-solute salts in RMB electrolytes.

owing to their lower melting points and reduced ion-ion interactions. Therefore, the free Li^+ ions in solution attract anions ionized from Mg salts, partially shielding the Mg^{2+}-anion electrostatic attraction and promoting Mg salt dissolution. As an example, adding $LiBH_4$ facilitates the dissociation of $Mg(BH_4)_2$, which greatly enhances the Coulombic efficiency and Mg plating/stripping kinetics of the $Mg(BH_4)_2$-DME electrolyte.[107] This improvement in electrochemical performance is primarily due to the increased concentration of free BH_4^- anion and the formation of a Mg–Li alloy interphase.[108,109] Zhang et al. demonstrated that incorporating LiCl increases $MgCl_2$ solubility and enables the formation of the active $[Mg_2(\mu\text{-}Cl)_3(THF)_6][LiCl_2(THF)_2]$ structure, which ensures a passivation-free electrolyte-electrode interphase and shortens the electrolyte's activation process.[110] Their further studies showed that the synergistic effect of LiHMDS and LiCl dual-salt additives facilitates the formation of a stable $[Mg_xLi_yHMDS_zCl_{2x+y-z}{\cdot}nTHF]$ solvation shell.[111] This structure reduces the Mg^{2+} de-solvation energy barrier via the anions' electric field effect and the lubrication effect of coordinated THF solvents. More importantly, these water-resistant and impurity-resistant aggregates allow Mg batteries to operate with 1000 ppm H_2O content and 97% $MgCl_2$ purity, significantly reducing RMBs commercialization costs. As a multi-functional additive, recent studies in LIBs have reported that LiHMDS promotes the formation of an electrochemically stable CEI layer and prevents the irreversible phase transformation of cathode materials, warranting further investigation in RMBs.[112] In addition to the aforementioned Li salts, other Li salts, LiOTf[113] and LiTFSI[114] salts have also been demonstrated to positively impact Mg electrolytes. Despite these advantages, the introduction of Li^+ into the Mg electrolyte will inevitably lead to the co-insertion of Li^+/Mg^{2+} dual-cations in cathode.[115] In contrast to traditional "rocking chair" batteries, these dual-ion batteries require a larger amount of electrolyte to achieve complete charge/discharge of the cathode material, posing challenges to achieving high energy density. Therefore, developing all-Mg salts electrolytes is vital.

Charge-delocalized anion structures (e.g., $TFSI^-$, ClO_4^-, $HMDS^-$, etc.) distribute the negative charge across the entire anionic group, reducing electrostatic interactions between Mg^{2+} cations and thereby exhibiting high solubility. Although pure ether solutions of these Mg salts tend to passivate the Mg anode, their combination with highly active $MgCl_2$ results in efficient all-Mg salts electrolytes. Aurbach et al. pioneered the development of the $Mg(TFSI)_2$-$MgCl_2$-DME electrolyte, wherein $Mg(TFSI)_2$ salts facilitate the dissolution of $MgCl_2$, while $MgCl_2$ enhances the electrolyte's electrochemical activity.[116] However, due to the lack of highly pure and anhydrous Mg salts, this electrolyte achieved only 80–90% Coulombic efficiency. The authors attributed this limited performance to side reactions and impurity accumulation on the Mg anode, and proposed the addition of Di-butyl Mg as an impurity scavenger. The modified electrolyte exhibited homogeneous Mg deposition behavior and a wide electrochemical window (>3 V). Additionally, the higher concentration of $MgCl_2$ in this electrolyte facilitates the formation of electroactive $[Mg_2Cl_3(THF)_6]^+$ cations, thereby improving its electrochemical performance.[48] Wang et al. reached similar conclusions, they reveal that the concentrated $Mg(TFSI)_2$-$MgCl_2$-DME electrolyte effectively reduces the solubility of sulfur and Mg polysulfides, thereby mitigating the shuttling effects. Additionally, its non-nucleophilic property contributes to the long-term cycling stability of Mg-S batteries.[117] Overall, benefiting from the facile preparation process and accessible raw materials, the $Mg(TFSI)_2$-$MgCl_2$ electrolyte has been widely used with organic materials,[118,119] sulfide,[120,121] and other cathode materials.

In addition to $Mg(TFSI)_2$-based electrolytes, other all-Mg salt electrolytes also exhibit excellent electrochemical stability. Zhang et al. developed an electrolyte by reacting perfluorinated tert-butoxide Mg salts ($Mg(Opftb)_2$) with $MgCl_2$, which features active $[Mg_2Cl_3{\cdot}6THF]^+$ cations and $[Mg(Opftb)_3]^-$ anions. The low LUMO energy level of this anion structure promotes its preferential decomposition during cycling, producing an organic-inorganic hybrid SEI layer. This robust SEI allows the Mg//Mg symmetrical cell to achieve an exceptional cycle life of 8100 h with a low overpotential of 75 mV.[122] Zhi Wei Seh et al. engineered an electrolyte containing $Mg(OTf)_2$ and $MgCl_2$, enabling uniform Mg deposition at a high current density of 3 mA cm^{-2} and a capacity of 5 mAh cm^{-2}.[123] Other charge-delocalized Mg salts, such as $Mg(HMDS)_2$,[124,125] Mg bis(diisopropyl)amide (MBA),[126] and $Mg(Ohfip)_2$[127] has also been demonstrated to significantly enhance the electrochemical performance of Mg electrolytes.

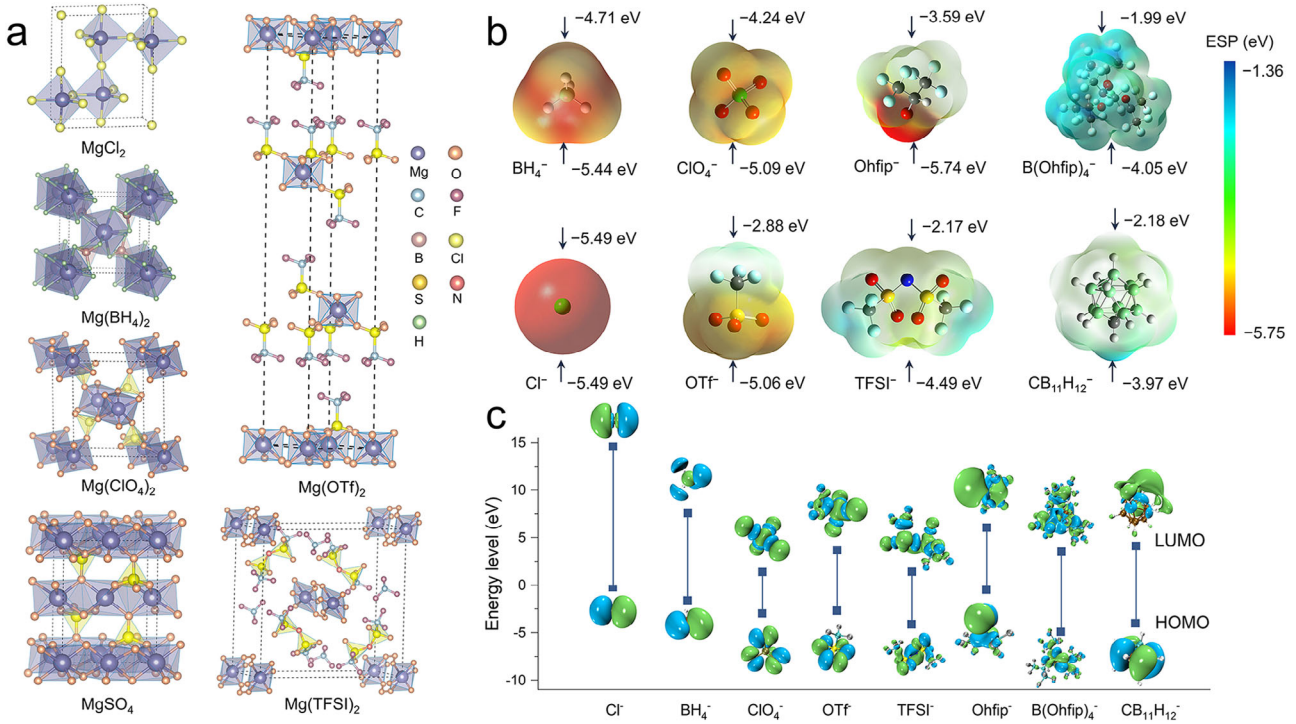

Figure 8. Structure and thermodynamic descriptors of common Mg salt anions. a) Crystal structures of common Mg salts, b) ESP mappings with the most negative and positive values of the anions from Mg salt; c) The HOMO and LUMO energies of these anions. The B3LYP functional combined with the 6–31G basis set in density functional theory was used for geometry optimization and energy calculation.

In summary, structurally and functionally diverse anion receptors have been introduced into Mg electrolytes. These anion receptors not only enable precise tailoring of electrolyte properties but also widen the electrochemical stability window and simultaneously enhance cycling stability through optimized interfacial chemistry and anion reconstruction, thereby playing an indispensable role in advancing RMB technologies.

4.3. Design Weakly Coordinated Anions

The development of functional active cations and anion receptors has enabled reversible Mg plating/stripping behavior in diverse electrolytes. However, most of these electrolytes rely on chlorine-containing formulations, where the presence of $Mg_xCl_y^+$ cations ensure high compatibility with Mg metal anodes. The high dissociation energy barrier of the Mg-Cl bond leads to high overpotentials when these electrolytes are paired with intercalation cathodes.[70,116] Additionally, the co-insertion of $MgCl^+$ cation hinders the two-electron transfer chemistry of the Mg/Mg^{2+} redox process and results in electrolyte consumption during battery cycling.[128,129] Therefore, the development of chlorine-free Mg electrolyte is widely recognized as the "holy grail" in RMBs research.

Most Mg salts exhibit a six-coordinated crystal structure, where Mg^{2+} is coordinated with six anions, forming a stable octahedral geometry with high lattice energy (**Figure 8a**). Therefore, dissolving Mg salts requires substantial energy to break the strong Mg^{2+}-anion bonds. Although the charge-delocalized anion structure enables the dissolution of Mg salts in ether-based solvents, the high charge density of Mg^{2+} leads to incomplete salt dissociation, facilitating the formation of tightly bonded CIPs within the electrolyte (such as $[Mg^{2+}\text{-}TFSI^-]$). Compared to free $TFSI^-$ anions, these Mg^{2+}-coordinated structures reduce the LUMO energy levels of the anions, making them more prone to reductive decomposition, which eventually passivates the Mg metal anode.[130–134] Electrostatic potential (ESP) maps provide insights into the surface charge distribution of molecules and can be used to quantify the binding strength of Mg^{2+} to anions. As shown in Figure 8b, the most negatives value among various Mg salts anions follow this sequence: $Ohfip^- < Cl^- < BH_4^- < ClO_4^- < OTf^- < TFSI^- < B(Ohfip)_4^- < CB_{11}H_{12}^-$, which corresponds to their binding affinity with Mg^{2+}. Among these, weakly coordinated anions, such as $B(Ohfip)_4^-$ and $CB_{11}H_{12}^-$, effectively mitigate strong electrostatic interactions with Mg^{2+}, and demonstrated enhanced intrinsic electrochemical stability (Figure 8c), making them promising candidates for high-voltage, passivation-free Mg electrolytes.

As early as 1990, a series of magnesium tetraorganoborate salts ($Mg(BR_4)_2$, R = butyl or phenyl) were reported.[71] When dissolved in THF, these electrolytes achieved efficient Mg plating/stripping and enabled reversible Mg^{2+} intercalation/extraction in Co_3O_4 cathodes. The researchers attributed this performance to the covalent nature and bulky structure of the anions, which enhanced ionic dissociation in solution. Although the low ionic conductivity of this electrolyte hinders its practical application, the anion structure presented in this study paves the way for designing chlorine-free, weakly coordinated Mg electrolytes. Inspired by this work, Mohtadi et al.

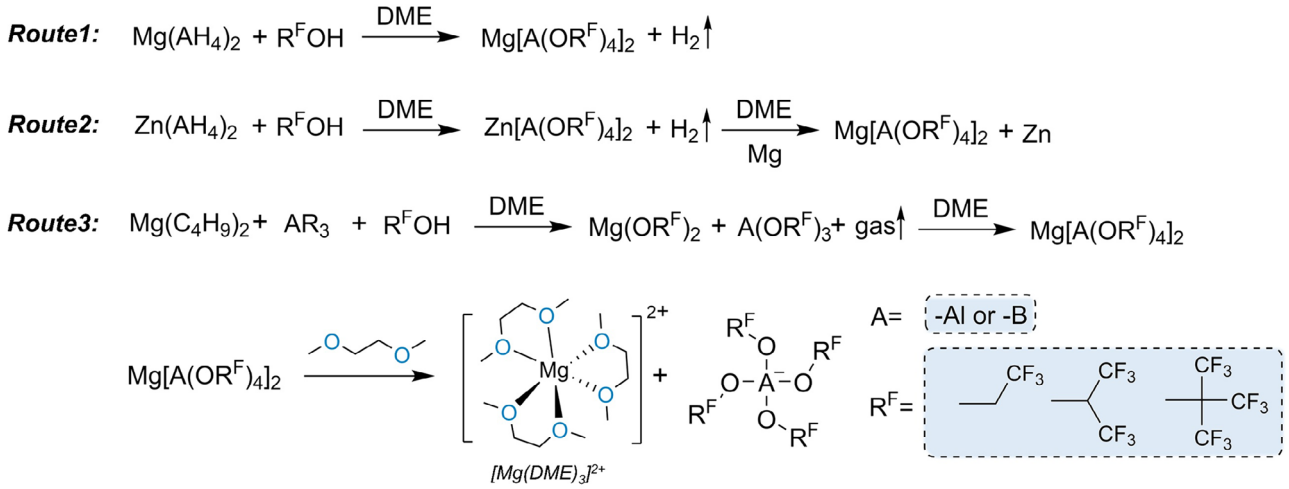

Scheme 3. Typical reaction routes of fluorinated Mg alkyloxyaluminate/alkyloxyborate salts.

reported that magnesium borohydride ($Mg(BH_4)_2$) enables reversible Mg plating/stripping in both THF and DME solvents.[107] However, due to its small anion size and insufficient charge delocalization, the electrolytes' ionic concentration and Coulombic efficiency remain uncompetitive. As discussed in the previous section, they introduced $LiBH_4$ as a co-solute to promote the $Mg(BH_4)_2$ dissociation, enhancing deposition current density by orders of magnitude. However, due to the β-H elimination reaction, these magnesium organoboron electrolytes all demonstrated insufficient oxidative stability (≈1.7 V of $Mg(BH_4)_2$, ≈1.77 V of $Mg(BPh_3Bu)_2$).[135] Muldoon et al. proposed the $Mg(BPh_4)_2$ and $Mg(BAr_F)_2$ (BAr_F = tetrakis[3,5-bis(trifluoromethyl)phenyl]borate) based electrolytes to improve oxidative stability by eliminating alkyl groups on the B center.[136] However, $Mg(BPh_4)_2$ exhibits a solubility of less than 0.01 M in THF, and $Mg(BAr_F)_2$ is not compatible with Mg metal anode.

The low oxidation stability of $Mg(BR_4)_2$-based electrolytes remained unresolved until 2017, when Zhao et al. addressed this issue by treating $Mg(BH_4)_2$ with various fluorinated alcohols to produce fluorinated Mg alkoxyborates ($Mg[B(OR^F)_4]_2$, R^F = fluorinated alkyl group) (**Scheme 3**).[137] Notably, the substitution of -H with hexafluoroisopropyl extends the oxidation stability of $Mg[B(Ohfip)_4]_2$-DME electrolyte to 4.3 V (**Figure 9a**). More importantly, the chlorine-free nature of this electrolyte allows this

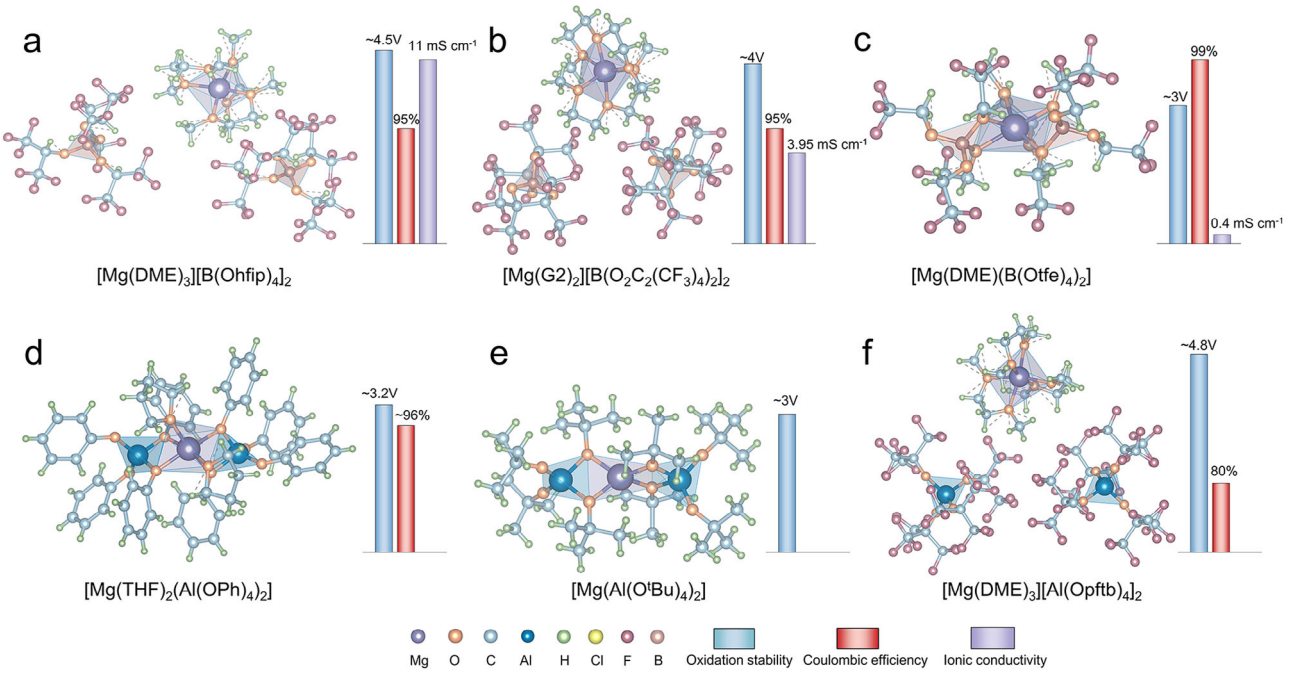

Figure 9. Single crystal structure and electrochemical properties of a) $[Mg(DME)_3][B(Ohfip)_4]_2$, b) $[Mg(G2)_2][B(O_2C_2(CF_3)_4)_2]_2$, c) $[Mg(DME)(B(Otfe)_4)_2]$, d) $[Mg(THF)_2(Al(OPh)_4)_2]$, e) $[Mg(Al(O^tBu)_4)_2]$, and f) $[Mg(DME)_3][Al(Opftb)_4]_2$.

enhanced oxidation stability to be maintained on Al or SS current collectors, significantly reducing the commercial application costs of RMBs. Their subsequent research optimized the synthesis process and improved the purity of $Mg[B(Ohfip)_4]_2$ salts. As a result, the highly purified $Mg[B(Ohfip)_4]_2$-DME electrolyte demonstrated even greater oxidation stability, reaching 4.5 V.[138] They identified 0.3 M as the optimal concentration for this electrolyte, which exhibits a high ionic conductivity comparable with Li-based electrolyte (11 mS cm^{-1} at 23 °C). With these remarkable properties, the $Mg[B(Ohfip)_4]_2$-DME electrolyte achieved long-term cyclability of up to 1200 h and delivered a high energy density of 1248 Wh kg^{-1} in Mg-S batteries. Although the same anionic structure was reported earlier in halogen-containing electrolytes, as we discussed in the previous section.[97] The direct synthesis of weakly coordinating $[B(Ohfip)_4]^-$ anions in pure Mg^{2+} electrolytes represents a critical advancement in the development of RMBs.

During the same period, the $Mg[Al(Ohfip)_4]_2$-DME electrolyte was also synthesized.[84] Unlike the alcohol substitution reactions used in the synthesis of $Mg[B(Ohfip)_4]_2$ salt, Arnold et al. employed $Al(Ohfip)_3$ as an anion receptor to react with $Mg(Ohfip)_2$ salt. The resulting $Mg[Al(Ohfip)_4]_2$ electrolyte exhibited reversible, high-efficiency Mg plating/stripping ability. Additionally, the $[Al(Ohfip)_4]^-$ anion demonstrated exceptional oxidation stability (>3.5 V), comparable to that of $[B(Ohfip)_4]^-$ anions, owing to the electron-withdrawing $-CF_3$ groups and the tetrahedral coordination structure. However, the Al-centered salts are exceptionally sensitive to moisture and decompose quickly upon exposure to air, requiring rigorous precautions throughout the preparation process. Building on this work, Mandai found that the $Mg[B(Ohfip)_4]_2$ electrolyte, prepared via the in situ reaction of $Mg(Ohfip)_2$, BH_3, and hexafluoroisopropanol (HFIP), demonstrated enhanced electrochemical properties than those prepared from $Mg(BH_4)_2$.[139] The key benefit of this transmetalation reaction is the removal of $Mg(BH_4)_2$ as a raw material, preventing the introduction of unwanted impurities such as MgH_2, MgX_2 (X = Cl or Br), and parent boron compounds during synthesis. More importantly, this work highlights two key challenges in RMB research. The first is the strong coordination between Mg^{2+} and DME molecules, which leads to solvent decomposition and the formation of an unfavorable electrode-electrolyte interphase during cycling. The second challenge is the uneven distribution of active sites on the Mg metal anode, resulting in isolated Mg deposits and ultimately leading to battery short circuits. These findings highlight the importance of designing Mg-ion conductive SEIs and substrates with high Mg affinity in advanced RMBs research.[140,141]

In addition to optimizing the synthesis process, a simple electrochemical "conditioning" process, similar to that used for the MACC electrolyte, allow the $Mg[B(Ohfip)_4]_2$ electrolyte (synthesized via the dehydrogenation reaction of $Mg(BH_4)_2$) to achieve improved Mg plating/stripping efficiency, reduced overpotential, and a more uniform Mg deposition morphology.[142] The enhanced electrochemical performances results from the elimination of detrimental contaminants and trace water. Similarly, the addition of 5 mM $Mg(BH_4)_2$ to the $Mg[B(Ohfip)_4]_2$ electrolyte helps eliminate the native oxide layer on the Mg metal anode and facilitates the formation of a stable SEI layer.[143] The enhanced performance of this electrolyte may also be attributed to the presence of BH_4^- ions, which effectively remove trace water in the electrolyte.[144] Apart from the purity of $Mg[B(Ohfip)_4]_2$ salts, the cost-effectiveness of synthesis process is another crucial consideration for the practical application of RMBs. A recent report described a cation replacement method for preparing $Mg[B(Ohfip)_4]_2$ salts from low-cost $Zn(BH_4)_2$ salts.[145] This simple method enables the production of $Mg[B(Ohfip)_4]_2$ salts on a hectogram scale and demonstrates the electrolyte's practical applicability in Mg-S pouch cells, achieving an energy density of 53.4 Wh kg^{-1}. While Zn^{2+} can be completely replaced by Mg^{2+} through cation exchange, using impure $Zn(BH_4)_2$ salts as raw material inevitably introduces undesirable impurities, such as NaCl. Thus, the resulting product requires further characterization to identify any additional impurity cations. Bitenc et al. systematically investigated how different synthesis processes affect the purity and electrochemical performance of $Mg[Al(Ohfip)_4]_2$ salts.[146] They found that Mg salts produced by cation exchange methods tend to retain substantial Na^+ residues, necessitating further purification. On the other hand, Mg salts synthesized through organometallic reactions show higher purity but at a higher cost. Overall, weakly coordinated $Mg[B(Ohfip)_4]_2$ and $Mg[Al(Ohfip)_4]_2$ are among the most promising Mg salts for next-generation Mg batteries. However, further research is required to develop cost-effective and high-purity synthesis methods for these electrolyte salts and to deepen the understanding of their compatibility with high-voltage cathodes.

Inspired by the great success of $Mg[B(Ohfip)_4]_2$ and $Mg[Al(Ohfip)_4]_2$ salts, several other weakly coordinated fluorinated Mg alkoxyborates/alkoxyaluminate anionic structures have been widely investigated. Liu et al. synthesized Mg perfluorinated pinacolatoborate (Mg-FPB) salts using a bidentate alkyloxide ligand, which precluded possible β-hydride elimination side reactions (Figure 9b).[147] Consequently, the Mg-FPB electrolyte exhibited enhanced Coulombic efficiency and reduced overpotential compared to the $Mg[B(Ohfip)_4]_2$ electrolyte, while also demonstrating excellent compatibility with high-voltage MnO_2 cathode. NuLi et al. developed a cost-effective Mg tetra(trifluoroethanoloxy)borate ($Mg[B(Otfe)_4]_2$) electrolyte (Figure 9c), delivering high oxidation stability (>3 V) and Coulombic efficiency (>99%).[148] Tan et al. designed an asymmetric B-centered anion by grafting $[OTf]^-$ onto $B(Otfe)_3$. The resulting weakly coordinated $[B(Otfe)_3OTf]^-$ structure prevents the passivation and decomposition of the $[Mg^{2+}\text{-}OTf^-]$ ion pair, ultimately enhancing the cycle stability and extending the lifespan of Mg batteries.[149] Grey et al. reported the synthesis of a series of $Mg[Al(OR)_4]_2$ (R = alkyl- or aryl-group) salts by employing $Mg(AlH_4)_2$ and various alcohols.[150] Their single-crystal X-ray and NMR analyses revealed that $Mg[Al(O^tBu)_4]_2$ and $Mg[Al(OPh)_4]_2$ salts exist as ion pairs in solution, suggesting that the absence of electron-withdrawing groups in the anion structures hinders the dissociation of the Mg salts (Figure 9d, e). On the contrary, the $Mg[Al(Opftb)_4]_2$ salt, with each anion containing 12 electron-withdrawing $-CF_3$ groups, is weakly coordinated, offering high solubility and enhanced Mg plating/stripping capability. Lau et al. draw a similar conclusion through comprehensive computational and electrochemical analyses on $Mg[Al(Opftb)_4]_2$ salts.[151] They found that this highly electron-deficient anionic structure weakens coordination with Mg^{2+}, preventing reduction-induced decomposition during

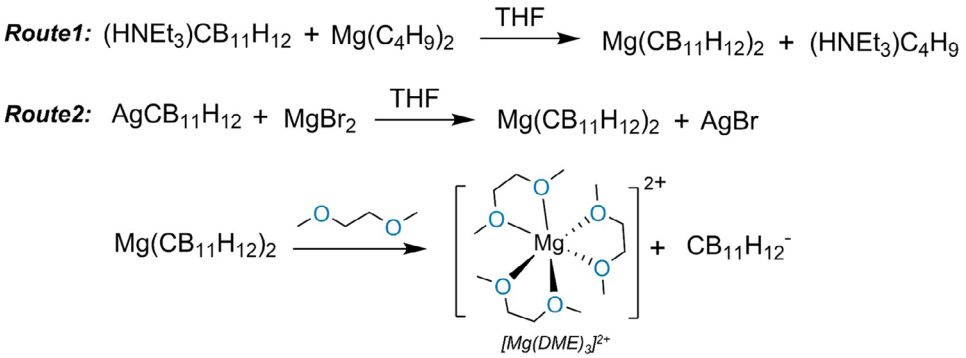

Scheme 4. Typical reaction routes of carborane-based Mg salts.

Mg^{2+} plating. As a result, the $Mg[Al(Opftb)_4]_2$ electrolyte exhibits both high reduction and oxidation stability (≈4.5 V vs Mg^{2+}/Mg). To gain a deeper understanding of how electron-withdrawing ligands improve the performance of weakly coordinated anionic structures, Bitenc et al. investigated the electrochemical behavior of Mg alkoxyborate electrolytes with different ligand fluorination degrees.[152] Their findings suggest that the perfluorinated $Mg[B(Opftb)_4]_2$ electrolyte is the optimal choice based on a comprehensive evaluation of electrolyte properties, including ionic conductivity, interfacial compatibility, and cycling stability. Additionally, they found that an inorganic boron-rich interphase plays a crucial role in achieving high Mg plating/stripping efficiency, low overpotential, and long-term cycling stability. A boron-rich cathode electrolyte interphase (CEI) is also considered beneficial for the Mg^{2+} de-solvation process and cross-interphase transfer.[153]

In summary, electron-withdrawing ligands, such as the —CF_3 group, are widely recognized for weakening the strong interactions between Mg^{2+} and anions. This effect facilitates the formation of weakly coordinated anionic structures, promotes Mg salt dissociation, and enhances the electrolyte's oxidation stability. However, the impact of excessive electron-withdrawing ligands (such as $Mg[Al(Opftb)_4]_2$ and $Mg[B(Opftb)_4]_2$ salts) on the Mg plating/stripping process remains controversial. Krossing et al. developed a chlorine-free synthesis method for $Mg[Al(Opftb)_4]_2$ salts (Figure 9f). Surprisingly, despite its high-purity, this electrolyte showed no electrochemical activity.[154] Their further experiments revealed that this phenomenon was due to the excessive use of —CF_3 ligands, which lowered the LUMO energy level of the anion (+3.36 eV). Although the electrolyte still demonstrated exceptionally high oxidation stability (>4 V), in line with previous reports by Grey and Lau et al.,[150,151] the significantly reduced LUMO energy level facilitated the reductive decomposition of this anion. As a result, an insulating MgF_2 layer (rutile structure) was formed, which hindered reversible chemical reactions. In contrast, the moderately fluorinated $Mg[Al(Ohfip)_4]_2$ and $Mg[B(Ohfip)_4]_2$ salts, with slightly higher LUMO energy levels (+3.42 and +4.17 eV, respectively), exhibited high electrochemical activity and reduction resistance.[155]

In addition to Al- and B-centered fluoride alkyl anions, carboranes represent another prominent class of weakly coordinated anions (**Scheme 4**). The first carborane anionic structure in Mg electrolyte was reported by Mohtadi et al.[156] The developed $[R_2MgCl]^-[Mg_2Cl_3]^+$ (R = 1-(1,7-$C_2B_{10}H_{11}$)) electrolyte (**Figure 10a**) exhibits a oxidation stability of 3.2 V, poor ionic conductivity (0.6 mS cm^{-1}), and decent Coulombic efficiency (98%). The chlorine-containing nature of this electrolyte drove them to design a more attractive, simpler Mg electrolyte. They attempted the synthesis of chlorine-free MgR_2 (R = 1-(1,7-$C_2B_{10}H_{11}$)) electrolyte, however, the attempt was failed due to its poor solubility. To further delocalize the anion's charge and achieve weak coordination, a monoanionic icosahedral $CB_{11}H_{12}^-$ structure was designed (Figure 10b).[157] In this structure, the negative charge of the anion is uniformly distributed within the cage bonding and fully delocalized across the cage. Besides, the absence of lone pairs of electrons allowed the $Mg(CB_{11}H_{12})_2$ salt to dissolve more effectively in ether solvents. Based on these distinct advantages, the $Mg(CB_{11}H_{12})_2$/G4 electrolyte exhibited an impressive oxidation stability of 3.8 V and a Coulombic efficiency exceeding 99%. However, the high viscosity and strong coordination of the long-chain G4 solvent hinder rapid Mg^{2+} diffusion in this electrolyte (ionic conductivity ≈1.8 mS cm^{-1}). To address this challenge, Yao et al. found that using short-chain DME/G2 (1:1, w/w) solvent blends improves Mg^{2+} diffusion kinetics while maintaining high salt solubility.[51] The resulting 0.5 mol kg^{-1} $Mg(CB_{11}H_{12})_2$/(DME-G2) electrolyte exhibited an enhanced ionic conductivity of 6.1 mS cm^{-1} and a superior Coulombic efficiency of 99.9%. These impressive transport properties enable homogenous and dendrite-free Mg plating behavior, even at a high current density of 50 mA cm^{-2}. When paired with a high-capacity pyrene-4,5,9,10-tetraone (PTO) cathode, the Mg battery demonstrated stable cycling over 200 cycles at 5 C (1C = 408 mA g^{-1}) and retained a high capacity of 210 mAh g^{-1} even at 50 C. This high-power (30.4 kW kg^{-1}), high-energy (313 Wh kg^{-1}) Mg battery prototype establishes a paradigm for next-generation multivalent metal-ion batteries.

Building on the great success of carborane anion $[CB_{11}H_{12}]^-$ in Mg electrolytes, several similar derivatives, including the 10-vertex closo-carborane anion $[CB_9H_{10}]^-$ (Figure 10c),[158] fluorinated carborane anion $[F\text{-}CB_{11}H_{11}]^-$,[159] halogenated carborane anions $[Br\text{-}CB_{11}H_{11}]^-$ and $[Cl\text{-}CB_{11}H_{11}]^-$,[160] alkyl-substituted carborane anion $[R\text{-}CB_{11}H_{11}]^-$ (R = C_5H_{11}) (Figure 10d),[161] and others,[162] have been developed for electrochemical performance optimization. Overall, carborane anions feature a 3D cage-like structure with highly delocalized charge, enabling them to tolerate high voltages while maintaining weak coordination with Mg^{2+}. These distinct properties allow carborane-based electrolytes to achieve high Mg^{2+} conductivity and excellent

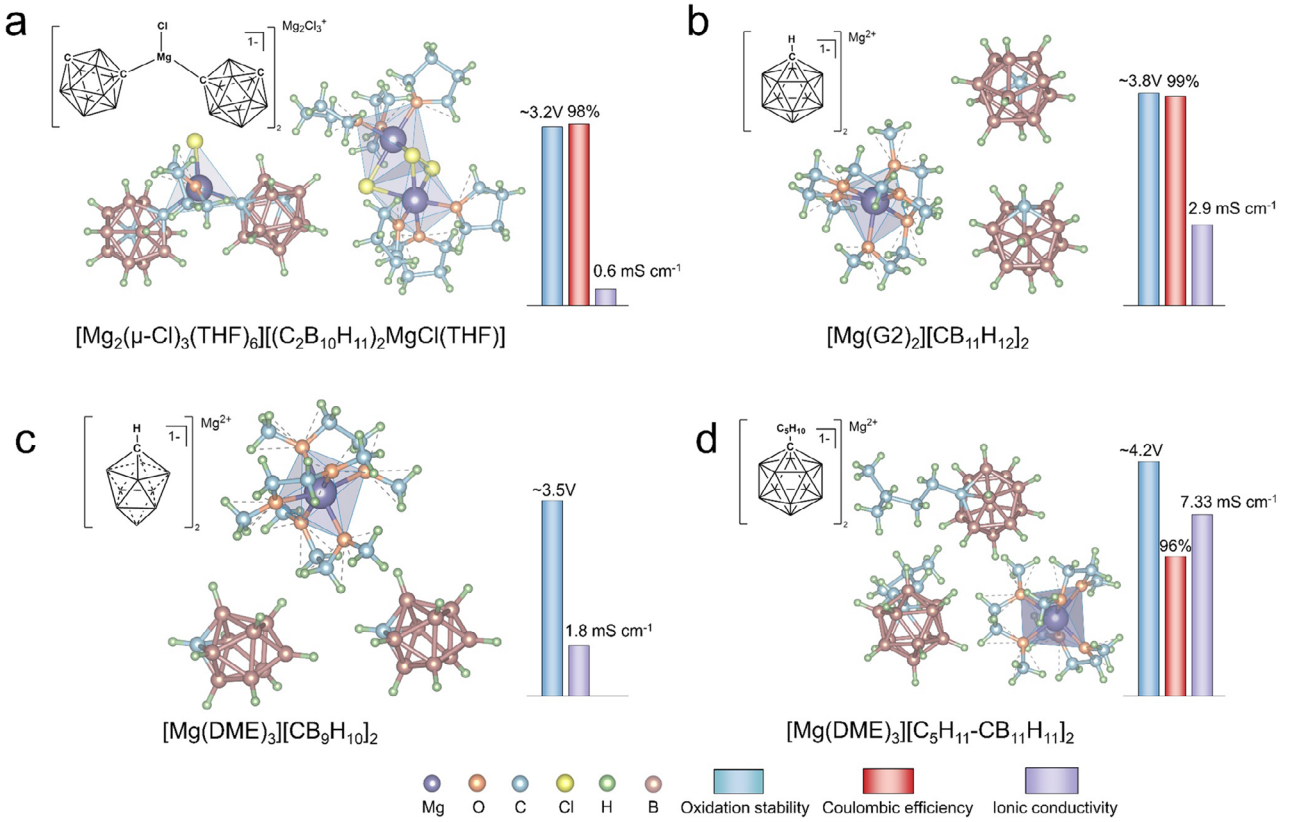

Figure 10. Single crystal structure and electrochemical properties of a) $[Mg_2(\mu\text{-}Cl)_3(THF)_6][(C_2B_{10}H_{11})_2MgCl(THF)]$, b) $[Mg(G2)_2][CB_{11}H_{12}]_2$, c) $[Mg(DME)_3][CB_9H_{10}]_2$, and d) $[Mg(DME)_3][C_5H_{11}\text{-}CB_{11}H_{11}]_2$.

compatibility with Mg anode, making them highly promising candidates for Mg electrolytes. To date, over 300 types of carborane anions have been identified, but only a few have been thoroughly studied in Mg electrolytes.[163] Therefore, further exploration of optimal structures is necessary. Moreover, the synthesis of carboranes is costly and complex, highlighting the urgent need for cost-effective and scalable production methods.

4.4. Design Solvation Structure

Recent progress in advanced characterization techniques, including in situ/ex situ spectroscopy (e.g., Raman, Fourier-transform infrared, NMR)[164] and computational modeling (molecular dynamics simulations and DFT),[165] has provided unprecedented insights into the dynamic evolution of solvation structures. These techniques have enabled researchers to better understand the relationship between solvation structures and battery performance at the molecular level. From a microscopic perspective, the solvation structure of Mg^{2+} influences de-solvation kinetics and ion transport, which in turn governs SEI composition and Mg deposition behavior. From a macroscopic perspective, the rational design of electrolyte components (solvent, salt, additives) facilitates the precise design of solvation environments, optimizing ionic conductivity, electrochemical stability, and interfacial compatibility. Therefore, optimizing the electrolyte performance by tailoring the solvation structure has gained increasing attention.[166]

Generally, the regulation of solvation structure in Mg batteries involves two main strategies (**Figure 11a**). The first strategy optimizes electrolyte components (solvent, co-solvent) to regulate the cations-solvent interaction, promoting the formation of anion-free, loose solvation structures. The second strategy focuses on regulating the interaction between cations and anions, facilitating the formation of anion-involved, passivation-free solvation structures. The mutual purpose of these strategies is to achieve highly reversible Mg plating/stripping (**Scheme 5**). Figure 11b depicts the solvation ability of various common Mg electrolyte solvents through ESP mappings. Solvents with lower most negative values, like TMP and TEP, promote the solvation of Mg^{2+}, leading to the formation of solvent-coordinated SSIP solvation structures. In contrast, solvents with higher most negative values, such as BTFE, are less prone to coordinate with Mg^{2+}, resulting in the formation of anion-involved solvation structures.

$Mg(TFSI)_2$ based electrolytes have been widely recognized to passivate the Mg metal anode.[48] However, rational engineering of their solvation structures can restore their electrochemical activity. Adding dimethylamine (DMA) co-solvent to the $Mg(TFSI)_2$-THF electrolyte enhances the solubility of Mg salts, resulting in the formation of a neutral $Mg(TFSI)_2(THF)_4$ solvation structure. This ion-pair structure reduces the charge density of solvated Mg^{2+}, promoting a faster de-solvation process.[167]Additionally, the amine solvent with stronger coordination ability preferentially coordinates with Mg^{2+}, leading to the formation of an anion-free solvation structure. Wang

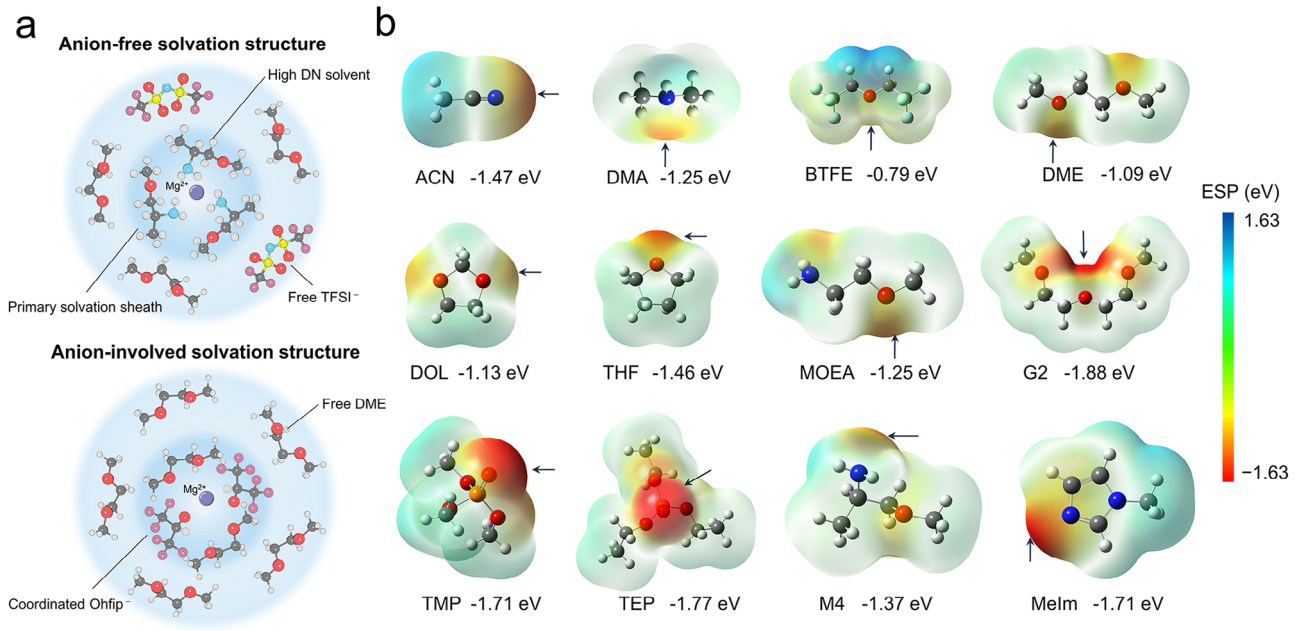

Figure 11. Illustration of solvation structure design. a) Local solvation structure of anion-free solvation structure and anion-involved solvation structure, b) ESP mappings with the most negative values of the commonly used organic solvents in RMB electrolytes.

et al. introduced a family of methoxyethyl-amine compounds into the $Mg(TFSI)_2$-DME electrolyte. Their stronger affinity with Mg^{2+} allows them to replace DME in the solvation sheath.[168] Compared with $[Mg^{2+}(DME)_3]$ (**Figure 12a**), the less compact $[Mg^{2+}(M4)_3]$ structure has a smaller solvation sheath reorganization energy, resulting in highly reversible Mg plating/stripping behavior and reduced overpotential. Additionally, the less compact structures enhance charge transfer kinetics in the layered oxide cathode. The assembled Mg-$Mg_{0.15}MnO_2$ battery demonstrated an impressive energy density of 412 Wh kg^{-1} and stable cycling over 200 cycles. Motivated by these pioneering findings, Zhao et al. further investigated the relationship between solvation structure and interfacial reactions in amine-based electrolytes.[169] They found that the $Mg(TFSI)_2$ electrolyte used 3-methoxypropylamine (S2) solvent achieves an optimal balance between the charge transfer process and the de-solvation process. This balance minimizes the reaction barrier on the anode interphase. Moreover, amines solvents show high water tolerance due to strong hydrogen bonding with water, enabling the assembled Mg batteries to maintain stable cycling even with up to 10,000 ppm water content. Even for the less solvated $Mg(OTf)_2$ salts (Figure 12b), amine reagents can effectively improve their solubility and electrochemical performance. Nuli and Tan reported a 2-methoxyethylamine (MOEA)/ether co-solvent $Mg(OTf)_2$-based electrolyte.[170,171] The strong solvent coordination effect of MOEA promotes the dissociation of the $[Mg\text{-}OTf]^+$

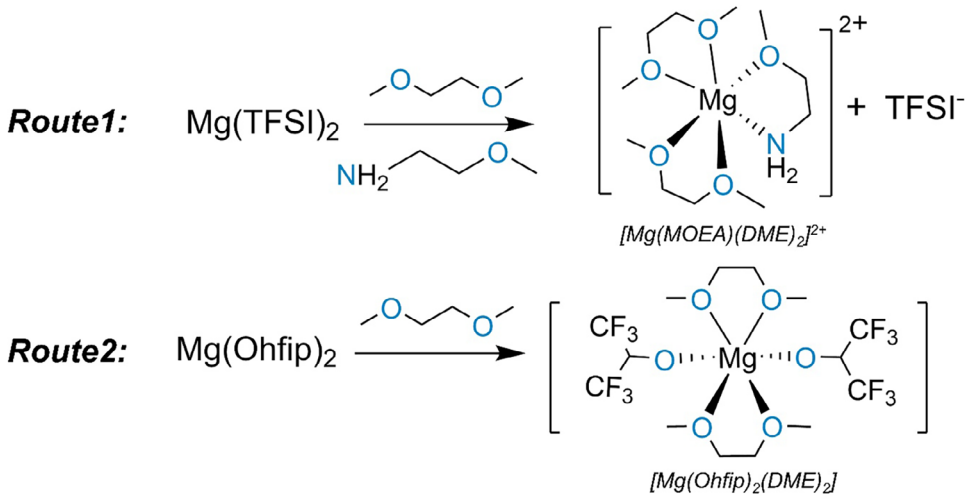

Scheme 5. Typical reaction routes of anion-free and anion-involved solvation structures.

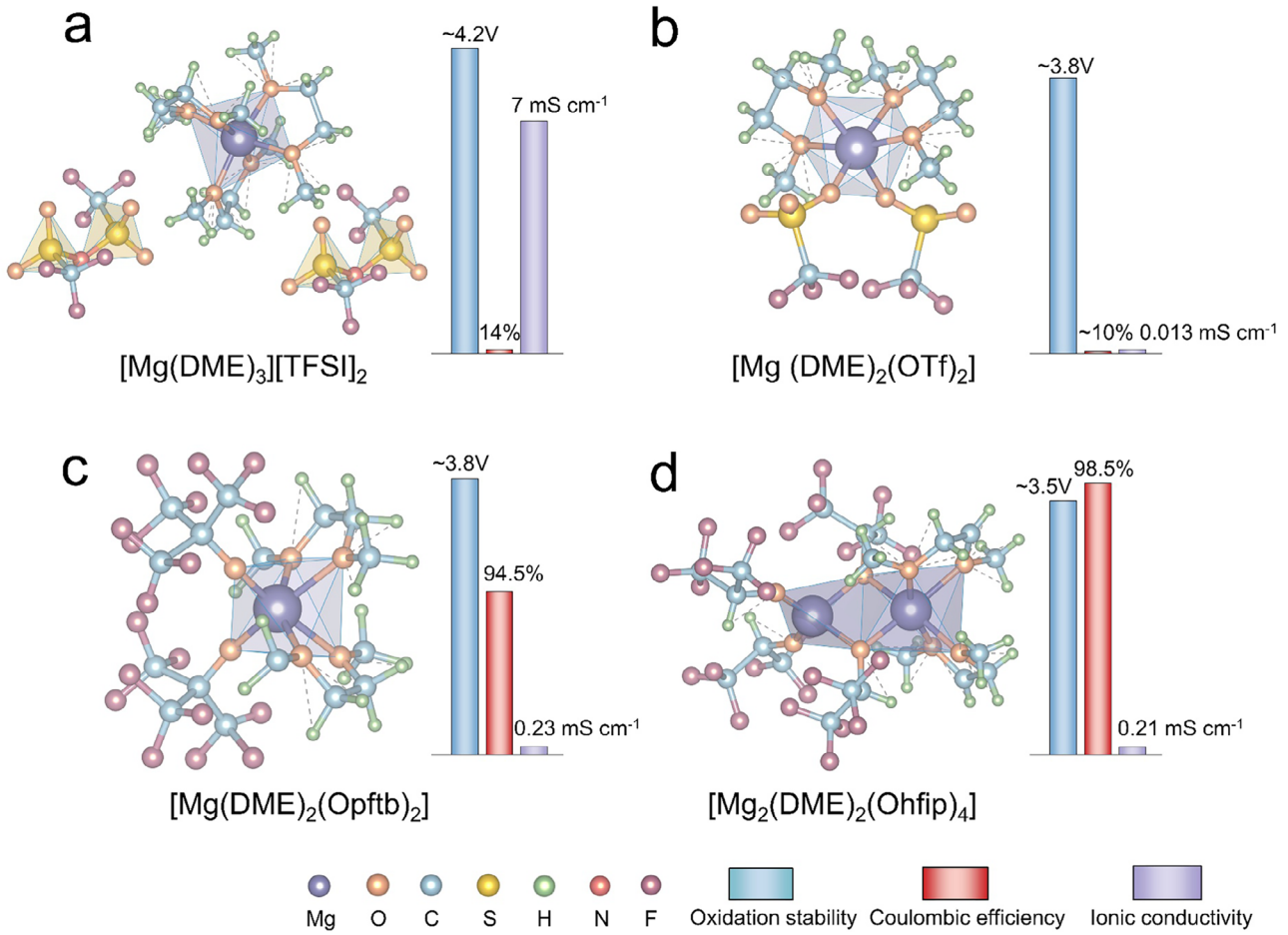

Figure 12. Single crystal structure and electrochemical properties of a) $[Mg(DME)_3][TFSI]_2$, b) $[Mg\ (DME)_2(OTf)_2]$, c) $[Mg(DME)_2(Opftb)_2]$, and d) $[Mg_2(DME)_2(Ohfip)_4]$.

ion pair and increases the population of (solvent-separated ion pairs) SSIPs in the electrolyte. This SSIP-dominated solvation structure increases both ionic conductivity and the reversibility of Mg plating/stripping. Furthermore, the preferred decomposition of MOEA-coordinated species results in the formation of a Mg_3N_2-rich gradient organic-inorganic SEI layer, enabling stable Mg//Mg symmetrical cell cycling for over 5000 h and Mg-Mo_6S_8 cell cycling for 1000 cycles. In addition to modifying solvation structures,[172] the partial ionization of amine/ether co-solvents in electrolyte can reduce the ion-pair content and generate active pseudo-Grignard reagent species, promoting the formation of a thin and passivation-free SEI.[173,174] Overall, amines reagents are widely used to regulate the solvation sheath of Mg^{2+} due to their unique nucleophilic amidogen ($-NH_2$) donor and high compatibility with Mg metal. However, their low oxidation stability and local adsorption on the Mg anode could present potential safety concerns, warranting further research.[175]

In addition to amines, which rely on high donor numbers (DN) to coordinate Mg^{2+}, ester solvents exhibit high polarity and a greater dipole moment. This enhances the ion-solvent ($U_{ion\text{-}dipole}$) interactions and promotes their participation in Mg^{2+} solvation structures. Introducing an appropriate amount of trimethyl phosphate (TMP) or triethyl phosphate (TEP) into the $Mg(TFSI)_2$-DME electrolyte transforms the compact $[Mg(DME)_3]^{2+}$ structure into $[Mg(DME)_2TMP]^{2+}$ or $[Mg(DME)_2TEP]^{2+}$ structures. These asymmetrical solvation sheaths facilitate the conversion of the DME decomposition-derived organic passivation layer into an organophosphorus-derived Mg^{2+}-conductive layer during cycling, enabling a reversible Mg metal anode.[176–178] Further, building on the TEP-modified $Mg(TFSI)_2$-DME electrolyte, Nazar et al. introduced an additional non-coordinating BTFE solvent as a diluent. The resulting electrolyte not only preserves the SSIPs-dominated solvation structure but also delivers enhanced ionic diffusion kinetics. Consequently, this co-ether phosphate electrolyte enables homogenous Mg plating/stripping for over 7000 h at a high current density of 2 mA cm^{-2}.[179] This innovative approach enhances both interfacial reaction kinetics (desolvation) and bulk-phase transport kinetics (ionic conductivity), providing new insights for the development of high-rate Mg batteries. Zhang et al. introduced methylimidazolium (MeIm) co-solvent to release free anions in $Mg(TFSI)_2$ and $Mg(HMDS)_2$-based electrolytes.[180] The high dielectric constants and donor number of MeIm allow it to easily coordinate with Mg^{2+}, reducing the content of CIPs and AGGs in the electrolyte. These released anions exhibit a higher LUMO energy level compared to paired anions, making them less prone to reduction and

decomposition, thus preventing passivation of the Mg anode during battery cycling. As a result, the electrolyte's ionic conductivity increases over 30 times, and the Mg//Mg symmetrical cell stably runs for over 800 h. Several other co-solvent formulations, such as DME-THF,[181,182] DME-B(Otfe)$_3$,[183] and THF-BTFE,[184] have also been demonstrated to facilitate the construction of favorable Mg^{2+} solvation structures.

While the aforementioned studies have shown that ion pairs in electrolytes lower LUMO energy levels, causing their decomposition at the interphase and passivation of the Mg anode, recent research has increasingly focused on strategies to rationally control cation-anion interaction strength and design anion-involved solvation structures.[185] Typically, in chlorine-containing electrolytes, the negatively charged halide species facilitates the de-solvation of solvated Mg^{2+}, therefore chlorine-containing electrolytes always exhibit superior Mg anode compatibility. Besides, introducing low charge delocalization $Mg(BH_4)_2$ salts into a $Mg(TFSI)_2$ electrolyte promotes the transformation of the solvation structure from $[Mg(TFSI)(G2)_2]^+$ to the neutral $[Mg(BH_4)(TFSI)(G2)]$ structure. During electrodeposition, the strongly bonded $[Mg(BH_4)]^+$ ion pair preferentially adsorbs onto the Mg anode, preventing the reduction and passivation of the $[Mg\text{-}TFSI]^+$ ion pair and ensuring highly reversible Mg plating and stripping.[186] Additionally, adding fluoride alkyl Mg salts ($Mg(Opftb)_2$) (Figure 12c) into a $MgCl_2$-$AlCl_3$-DME electrolyte facilitates the formation of neutral $[MgCl(Opftb)(DME)_2]$ solvation structure. This structure promotes the in situ formation of a stable, anion-derived MgF_2-rich SEI layer during cycling, which allows the Mg battery to maintain a superior Coulombic efficiency of 99.5% over 3000 cycles.[187] Besides, the addition of NaOTf to a $Mg[B(Ohfip)_4]_2$-DME electrolyte transforms the solvation structure into $[Mg(DME)_{2.5}OTf]^+$, which results in a lower Mg^{2+} de-solvation barrier and faster reaction kinetics on the CuSe cathode.[188] In addition to introducing salts to coordinate with Mg^{2+}, increasing the electrolyte concentration to minimize free solvent content can also lead to a CIPs-dominated solvation structure. The 2 M $Mg(Ohfip)_2$-DME electrolyte demonstrated highly efficient Mg plating/stripping and excellent cathode compatibility (Figure 12d), owing to the abundant active $[Mg\text{-}Ohfip]^+$ ion pairs within the electrolyte. These ion pairs mitigate the charge density of Mg^{2+} and facilitate a rapid de-solvation process.[52] Besides, the use of $Mg(OTf)_2$ salts with moderate charge delocalization promotes the formation of anion-involved solvation structures in strongly coordinated amine or ester solvents.[189] The anion-cation interactions within the solvation sheath reduce the bonding between Mg^{2+} and the solvent, thereby preventing the dehydrogenation decomposition of the -NH_2 group,[190] and promoting the formation of an anion-derived inorganic-rich SEI.[191] Additionally, the decomposition of free OTf^- anions promotes the formation of a C_xN_y and MgF_2-enriched CEI interphase, ensuring favorable cathode compatibility.[192] Building on these research findings, we can conclude that solvated cations, including SSIPs, CIPs, and AGGs, is more likely to reduction on the anode surface, thereby significantly influencing the evolution of the SEI interphase. In contrast, free anions and the solvent, which are more prone to oxidation on the cathode surface, govern the composition of the CEI interphase. By rationally regulating the electrolyte components, the ionic insulating passivation layer can be converted into a favorable SEI/CEI interphase.

In addition to regulating the solvation structure of the bulk electrolyte, precisely controlling the local solvation environment presents another way for a highly reversible Mg metal anode.[193] The introduction of isobutylamine (IBA) and $Mg(Bu)_2$ additives to the $Mg(TFSI)_2$/G2 electrolyte promotes the formation of a H_2O-free solvation structure, thereby protecting the Mg metal from surface passivation induced by trace H_2O.[173] The addition of 1-chloropropane (CP) to the $Mg(OTf)_2$/DME electrolyte enables a Cl-rich SEI interphase, thus facilitating the homogenous Mg(002) plane plating.[194] In addition, $TBABH_4$ and TBAOTf, as multifunctional electrolyte additives, not only eliminate trace H_2O, promoting a robust inorganic SEI interphase,[124,144,195] but also balance the interfacial Mg^{2+} diffusion-reduction rate, which enables long-life RMBs.[127]

Overall, the solvation structure serves as the electrolyte's "microscopic gene", directly influencing ion transport, interfacial reactions, electrochemical stability, and deposition behavior. By modulating the solvation structure, the "gene expression" of the electrolyte can be optimized, paving the way for high-performance Mg batteries.

5. Summary and Outlook

In summary, RMBs have emerged as a promising candidate for next-generation energy storage technologies due to their abundant resources, inherent safety, and high theoretical capacity. This review highlights recent breakthroughs in nonaqueous Mg electrolytes, specifically focusing on the design of active cations, anion receptors, weakly coordinated anions, and solvation structure. **Table 2** presents a detailed summary of the electrochemical performance of typical RMB electrolytes. As indicated, the development of active cations and anion receptors in chlorine-containing electrolytes enhances their compatibility with Mg anodes. However, their corrosive nature compromises both electrochemical stability and cathode compatibility, preventing them from meeting the increasing demand for high-voltage RMBs. On the other hand, the design of weakly coordinated anions ensures the Mg electrolyte exhibits high ionic conductivity, a broad electrochemical window, and good anode/cathode compatibility. However, their high cost and complex synthesis processes restrict their large-scale application. While simple Mg salt electrolytes offer greater practical potential, their low ionic conductivity makes them prone to inducing passivation of the Mg anode (**Figure 13**). Future research on Mg electrolytes should prioritize the design of weakly coordinated anions and the optimization of Mg^{2+} solvation in simple salt electrolytes to improve electrolytes' plating/stripping capacity and cathode compatibility. This review provides a comprehensive understanding of the fundamental solvent-salt interactions in Mg electrolytes, which is expected to drive the development of high-performance RMBs.

Despite significant advancements made in this field, several challenging yet promising directions remain, as detailed follow:

1) High-purity Mg Salts Production Techniques. The purity of Mg salts significantly influences the Coulombic efficiency, solubility, and cycle stability of the electrolyte. In particular, for chlorine-free electrolytes, trace amounts of water or impurities can passivate the Mg metal anode.[173] Moreover, since

Table 2. Summary of electrochemical performances for typical RMB electrolytes.

Electrolyte	Oxidation stability [V]	Conductivity [ms cm^{-1}]	Coulombic efficiency	Cycle life [h]	Matched cathode	Cyclability [retention]	Refs.
2.5 M C_2H_5MgBr/Et_2O	<2.0 V	low	≈71%	/	/	/	[49]
0.25 M $Mg(AlCl_2BuEt)_2$/THF	≈2.5 V (Pt)	≈5	≈100%	/	Mo_6S_8	2000 (85%)	[21]
0.4 M $MgCl_2$+$AlCl_2Et$/DME	≈3.0 V (Pt)	4.1	≈95%	400h	Mo_6S_8	75	[59]
0.3 M $MgCl_2$+$AlCl_3$ +PYR14TFSI/THF	≈2.5 V (SS)	8.5	≈100%	50h	S	20	[62]
0.4 M PhMgCl+ $AlCl_3$/THF (APC)	≈3.2 V (Pt)	≈4	≈100%	/	Mo_6S_8	94 (100%)	[72]
0.25 M $MgCl_2$+ $AlCl_3$/DME (MACC)	≈3.1 V (Pt)	≈2	≈99%	30h	Mo_6S_8	15	[74]
0.4 M HMDSMgCl+$AlCl_3$/THF	≈3.2 V (Pt)	≈2	≈100%	/	S	2	[75]
0.67 M $MgCl_2$+$AlEtCl_2$/THF	≈2.9 V (GC)	6.99	≈100%	/	Mo_6S_8	100 (95%)	[86]
0.5 M $Al(OPh)_3$+PhMgCl/THF	≈5.0 V (Pt)	1.24	≈98%	96h	WSe_2	50	[87]
0.4 M Mes_3B+PhMgCl/THF	≈3.5 V (Pt)	2	≈100%	600h	Mo_6S_8	50	[50]
0.2 M $MgCl_2$+ $B(OPh)_3$+TPFPB/THF	≈3.0 V (Mo)	/	≈98%	300h	Mo_6S_8	50	[95]
0.5 M $MgCl_2$+ $B(Ohfip)_3$+Mg/DME	≈3.3 V (Pt)	5.58	≈98%	700h	S	100 (80%)	[99]
0.05 M MgF_2+$B(Ohfip)_3$/DME	≈3.8 V (Al)	1.1	≈99%	/	Se	200	[97]
0.24 M I_2+$B(Ohfip)_3$+Mg/DME	≈3.8 V (Mo)	11	≈98%	1500h	Mo_6S_8	1200 (81.6%)	[100]
0.5 M $MgCl_2$+$B(Otfe)_3$/THF	≈3.0 V (Pt)	/	≈94%	120h	Mo_6S_8	100	[101]
0.4 M $Mg(OTf)_2$+$InCl_3$/DME	/	/	≈98%	600h	Mo_6S_8	800 (95%)	[105]
1.0 M $MgCl_2$+$Mg(TFSI)_2$/DME	>3.0 V (Pt)	/	≈93%	/	S	100 (69%)	[117]
1.2 M $MgCl_2$+$Mg(Opftb)_2$/THF	≈3.1 V (Pt)	/	≈99%	8100h	Mo_6S_8	800	[122]
0.4 M $MgCl_2$+$AlCl_3$+ $Mg(Opftb)_2$/DME	≈3.8 V (Mo)	/	≈99%	2000h	Mo_6S_8	500 (93%)	[187]
0.1 M $Mg(BH_4)_2$/DME	≈1.7 V (Pt)	/	≈67%	/	Mo_6S_8	40	[107]
0.3 M $Mg[B(Ohfip)_4]_2$/DME	≈4.5 V (Pt)	11	≈95%	1200h	S	100	[138]
0.25 M $Mg[Al(Ohfip)_4]_2$/DME	≈3.5 V (GC)	6.5	≈99%	/	Mo_6S_8	50	[84]
0.5 M $Mg[B(O_2C_2(CF_3)_4)_2]_2$/G2	≈4.0 V (SS)	3.95	≈95%	500h	MnO_2	/	[147]
0.75 M $Mg[B(Otfe)_4]_2$/THF	≈3.0 V (SS)	0.4	≈99%	200h	Mo_6S_8	210	[148]
0.4 M $Mg[Al(Opftb)_4]_2$/G3	≈4.8 V (Au)	3.1	≈80%	/	/	/	[151]
0.5 M $Mg(CB_{11}H_{12})_2$/DME-G2	≈3.8 V (Al)	6.1	≈100%	83h	PTO	700	[51]
0.75 M $Mg(CB_9H_{10})_2$/G4	≈3.5 V (Pt)	1.8	/	/	Mo_6S_8	30	[158]
0.9 M $Mg(C_5H_{11}$-$CB_{11}H_{11})_2$/DME	≈4.2 V (Pt)	7.33	≈96%	400h	Mo_6S_8	60	[161]
0.5 M $Mg(TFSI)_2$/DME-M4	≈3.8 V (SS)	4	≈99%	180h	$Mg_{0.15}MnO_2$	200	[168]
0.1 M $Mg(TFSI)_2$/S2	≈2.7 V (SS)	0.94	≈95%	350h	Mo_6S_8	100	[169]
0.25 M $Mg(OTf)_2$/G2-MOEA	≈2.8 V (SS)	≈0.7	≈98%	5000h	Mo_6S_8	1000 (89%)	[171]
0.4 M $Mg(TFSI)_2$/DME-G2-BTFE-TEP	≈4.1 V (Al)	2.8	≈95%	7000h	PANI	400 (72%)	[179]
0.3 M $Mg(TFSI)_2$/DME-MeIm	≈3.0 V (Al)	8.3	≈90%	800h	Mo_6S_8	120	[180]
2 M $Mg(Ohfip)_2$/DME	≈3.5 V (SS)	0.2	≈98%	300h	PDI-EDA	400 (80%)	[52]
0.5 M $Mg(OTf)_2$/G2-TMP	/	0.75	≈98%	3000h	PTCDI	40	[191]

research on Mg batteries is still in its infancy, novel Mg salts synthesized in different laboratories may contain impurity cations or halogens, leading to performance variations and inconsistent conclusions.[146] Therefore, detecting impurity elements and develop low-cost, high-purity Mg salts synthesis technique is essential.

2) Investigating the Practical Stability Limits of Mg Electrolytes. Achieving high energy density in Mg batteries requires the development of high-voltage cathode materials and electrolytes with a wide electrochemical window. Although numerous Mg electrolytes exhibit excellent oxidation stability (>3 V) on inert current collectors, their practical use in full cells remains constrained to low-voltage (≈2 V) cathodes, such as Mo_6S_8 and CuS. This limitation may arise from the inherent instability of electrolytes within porous electrodes.[196] Therefore, future linear sweep voltammetry (LSV) tests of Mg electrolytes

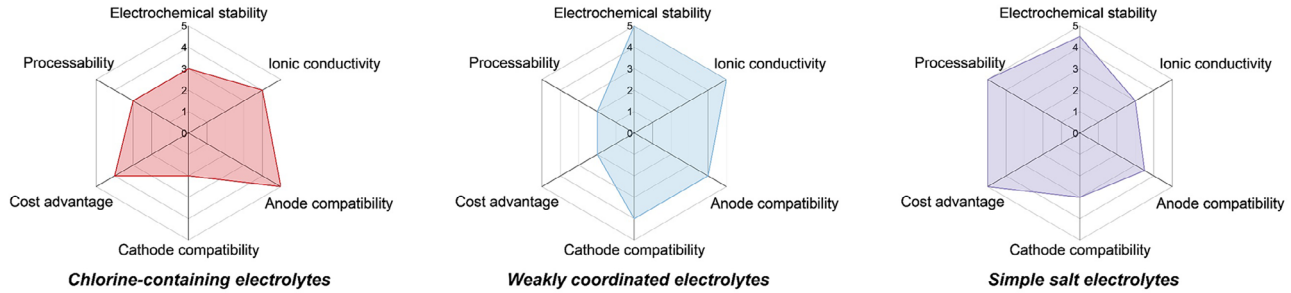

Figure 13. Comparison of the key parameters of various Mg electrolytes, including chlorine-containing electrolytes, weakly coordinated electrolytes, and simple salt electrolytes. The evaluation criteria for the electrochemical stability and ionic conductivity are derived from the electrochemical performance of various electrolytes presented in Table 2. The criteria for cathode and anode compatibility are based on the de-solvation process, interphase compatibility, and cycle life of different electrolytes. The criteria for cost advantage and processability are based on the cost and synthesis process steps of the electrolytes.

should include an investigation of the practical stability limits on porous materials.

3) Clarifying the design principles of RMB electrolytes. The interactions between ions and molecules in bulk electrolytes determine the microscopic solvation structure. Typically, introducing anion receptors and strong polar solvents reduces the content of CIPs and AGGs in the electrolyte, promoting rapid ion diffusion. However, the relationship between the solvation structure, interphase decomposition reactions, and interphase ion transport mechanisms remain unclear. Future electrolyte design should focus on both cathode/anode interphase compatibility to obtain a more promising RMB prototype.
4) Focus on the anion-solvent interaction. The dissolution of certain Mg salts in nonaqueous solvents remain challenging due to strong Mg-anion interactions. Previous studies focused on designing anion acceptors or weakly coordinated anions to reduce these interactions. Besides, nucleophilic aprotic solvents are predominantly employed in Mg electrolytes, which significantly reduce the anions' solvation effect. Although anions are poorly solvated in ether or amine-based solvents, solvents with exposed positive charge sites are expected to enhance the anion-solvent interactions, facilitating the dissolution of Mg salts. Most importantly, anion-solvent interactions can enhance the reductive stability of solvents, thereby suppressing side reactions at the interphase. Additionally, these interactions limit anion mobility, enhancing the cation transference number and improving the battery's rate capability. While pioneering work has been conducted in this area,[197,198] further research remains necessary.
5) Designing multifunctional RMB electrolytes. Current RMB electrolytes are limited by strict usage requirements, such as room-temperature operation, reliance on ultrahigh-purity salts, and stringent water content control at ppm levels. These constraints restrict their suitability for extreme environments and cost-effective manufacturing. The development of multifunctional RMB electrolytes with a wide operating temperature range (−40 to 80 °C), resistance to water and impurities will not only broaden the potential applications of RMBs but also reduce production costs, providing a significant competitive advantage.
6) Developing Emerging Solvents and Additives. Ether-based solvents (such as THF, DME) continue to be the dominant choice for Mg electrolytes. While amine solvents have gained attention, their limited oxidative stability remains a concern. Meanwhile, fluorinated ethers and additives, which have garnered significant interest in lithium electrolyte,[199] deserve further exploration for Mg battery applications. Additionally, electrolyte systems like weakly solvated electrolytes, high-concentration electrolytes, localized high-concentration electrolytes, and solid-state electrolytes[200] represent promising avenues for the further development of Mg batteries.[30]
7) In situ Characterization Tools and Machine Learning Methods. Compared to monovalent ions (Li^+, Na^+, K^+), the dissolution and association behaviors of divalent Mg^{2+} in solvents are more complex and involve multiple steps, leading to the formation of more intricate CIPs or AGGs. The development of in situ characterization techniques is therefore essential for uncovering the relationship between electrolytes' microstructure and their bulk properties. Furthermore, the integration of advanced optimization algorithms (e.g., Bayesian optimization, genetic algorithms) with machine learning models facilitates the identification of optimal electrolyte formulations from vast chemical libraries, significantly reducing the reliance for conventional trial-and-error methods. In the future, combining in situ characterization techniques with AI-driven simulations (e.g., molecular dynamics and machine learning) will enable precise control of solvation chemistry, accelerating electrolyte development cycles, reducing costs, and enhancing performance.[201]

Overall, advanced Mg electrolyte design necessitates not only careful compositional engineering but also the strategic modulation of intermolecular interactions. Future research should integrate multiscale modeling, in situ characterization, and solvation regulation to develop electrolytes that improve Mg plating uniformity, oxidation stability, interphase compatibility, and rapid desolvation kinetics, thereby unlocking the full potential of multivalent Mg-based energy storage systems.

Acknowledgements

This work was supported by the National Key Research and Development Program of China (No. 2023YFB3809501), the National Natural Science Foundation of China (52472246).

Conflict of Interest

The authors declare no conflict of interest.

Keywords

nonaqueous electrolytes, rechargeable magnesium batteries, solvation chemistry

Received: June 3, 2025
Revised: July 5, 2025
Published online:

[1] Y. S. Meng, V. Srinivasan, K. Xu, *Science* **2022**, *378*, abq3750.
[2] J. Xu, J. Zhang, T. P. Pollard, Q. Li, S. Tan, S. Hou, H. Wan, F. u. Chen, H. He, E. Hu, K. Xu, X.-Q. Yang, O. Borodin, C. Wang, *Nature* **2023**, *614*, 694.
[3] G. Xiao, H. Xu, C. Bai, M. Liu, Y.-B. He, *Interdisciplinary Materials* **2023**, *2*, 609.
[4] K. N. Wood, E. Kazyak, A. F. Chadwick, K.-H. Chen, J. i.-G. Zhang, K. Thornton, N. P. Dasgupta, *ACS Cent. Sci.* **2016**, *2*, 790.
[5] J. Wei, P. Zhang, J. Sun, Y. Liu, F. Li, H. Xu, R. Ye, Z. Tie, L. Sun, Z. Jin, *Chem. Soc. Rev.* **2024**, *53*, 10335.
[6] L. Cui, S. Zhang, J. Ju, T. Liu, Y. Zheng, J. Xu, Y. Wang, J. Li, J. Zhao, J. Ma, J. Wang, G. Xu, T.-S. Chan, Y.-C. Huang, S.-C. Haw, J.-M. Chen, Z. Hu, G. Cui, *Nat. Energy* **2024**, *9*, 1084.
[7] K. Wang, Y. Wang, J. Wang, H. Wang, C. Ding, Z. Zheng, Y. Liu, Z. Luo, Y. Ding, *Adv. Funct. Mater.* **2025**, *35*, 2422689.
[8] S. Rao, R. Wu, Z. Zhu, J. Wu, Y. Ding, L. Mai, *Nano Energy* **2023**, *112*, 108462.
[9] L. Li, R. Wu, H. Ma, B. Cheng, S. Rao, S. Lin, C. Xu, L. Li, Y. Ding, L. Mai, *Small* **2023**, *19*, 2300762.
[10] M. Li, S. Yang, B. Li, *Interdisciplinary Materials* **2024**, *3*, 805.
[11] Z. Huang, T. Wang, X. Li, H. Cui, G. Liang, Q. i. Yang, Z. e. Chen, A. o. Chen, Y. Guo, J. Fan, C. Zhi, *Adv. Mater.* **2022**, *34*, 2106180.
[12] H. Chen, Y. Zhao, X. Zhang, R. Li, A. Wang, H. Zhang, J. Liu, B. Wen, L. Zhang, Q. Hua, T. Liu, K. Wu, K. Amine, J. Luo, *Nature Synthesis* **2025**, *4*, 552.
[13] C. Sun, H. Wang, F. Yang, A. Tang, G. Huang, L. Li, Z. Wang, B. Qu, C. Xu, S. Tan, X. Zhou, J. Wang, F. Pan, *J. Magnesium Alloys* **2023**, *11*, 840.
[14] Y. Liang, H. Dong, D. Aurbach, Y. Yao, *Nat. Energy* **2020**, *5*, 646.
[15] F. Liu, G. Cao, J. Ban, H. Lei, Y. Zhang, G. Shao, A. Zhou, L. Z. Fan, J. Hu, *J. Magnesium Alloys* **2022**, *10*, 2699.
[16] X. Liu, A. Du, Z. Guo, C. Wang, X. Zhou, J. Zhao, F. u. Sun, S. Dong, G. Cui, *Adv. Mater.* **2022**, *34*, 2201886.
[17] J. Zhang, Z. Chang, Z. Zhang, A. Du, S. Dong, Z. Li, G. Li, G. Cui, *ACS Nano* **2021**, *15*, 15594.
[18] S. Riedel, L. Wang, M. Fichtner, Z. Zhao-Karger, *Chemistry – A European Journal* **2024**, *30*, 202402754.
[19] G. Han, Y. Lu, H. Jia, Z. Ding, L. Wu, Y. Shi, G. Wang, Q. Luo, Y. u. Chen, J. Wang, G. Huang, X. Zhou, Q. Li, F. Pan, *J. Magnesium Alloys* **2023**, *11*, 3896.
[20] X.-F. Ma, H.-Y. i. Li, J. Tan, J. Wang, J. Diao, J. Yue, S. Tan, G. Huang, J. Wang, F. Pan, *J. Magnesium Alloys* **2025**, *13*, 1592.
[21] D. Aurbach, Z. Lu, A. Schechter, Y. Gofer, H. Gizbar, R. Turgeman, Y. Cohen, M. Moshkovich, E. Levi, *Nature* **2000**, *407*, 724.
[22] K. W. Leong, W. Pan, X. Yi, S. Luo, X. Zhao, Y. Zhang, Y. Wang, J. Mao, Y. Chen, J. Xuan, H. Wang, D. Y. C. Leung, *Sci. Adv.* **2023**, *9*, adh1181.
[23] S.-B. Son, T. Gao, S. P. Harvey, K. X. Steirer, A. Stokes, A. Norman, C. Wang, A. Cresce, K. Xu, C. Ban, *Nat. Chem.* **2018**, *10*, 532.
[24] J. Muldoon, C. B. Bucur, A. G. Oliver, T. Sugimoto, M. Matsui, H. S. Kim, G. D. Allred, J. Zajicek, Y. Kotani, *Energy Environ. Sci.* **2012**, *5*, 5941.
[25] D. Aurbach, G. S. Suresh, E. Levi, A. Mitelman, O. Mizrahi, O. Chusid, M. Brunelli, *Adv. Mater.* **2007**, *19*, 4260.
[26] F. Liu, T. Wang, X. Liu, L.-Z. Fan, *Adv. Energy Mater.* **2021**, *11*, 2000787.
[27] H. Shuai, J. Xu, K. Huang, *Coord. Chem. Rev.* **2020**, *422*, 213478.
[28] Y. Li, S. Guan, H. Huo, Y. Ma, Y. Gao, P. Zuo, G. Yin, *Adv. Funct. Mater.* **2021**, *31*, 2100650.
[29] J. Muldoon, C. B. Bucur, T. Gregory, *Angew. Chem., Int. Ed.* **2017**, *56*, 12064.
[30] P. Xiao, X. Yun, Y. Chen, X. Guo, P. Gao, G. Zhou, C. Zheng, *Chem. Soc. Rev.* **2023**, *52*, 5255.
[31] X. Chen, Q. Zhang, *Acc. Chem. Res.* **2020**, *53*, 1992.
[32] A. Benmayza, M. Ramanathan, T. S. Arthur, M. Matsui, F. Mizuno, J. Guo, P.-A. Glans, J. Prakash, *J. Phys. Chem.* **2013**, *117*, 26881.
[33] L. Xue, Y. Li, H. Gao, W. Zhou, X. Lü, W. Kaveevivitchai, A. Manthiram, J. B. Goodenough, *J. Am. Chem. Soc.* **2017**, *139*, 2164.
[34] H. Kim, M. Deng, A. Fortuin, T. Würger, P. Georgopanos, D. Kramer, M. Zheludkevich, D. Höche, *Adv. Energy Mater.* **2024**, *14*, 2401266.
[35] Z. Li, H. Rao, R. Atwi, B. M. Sivakumar, B. Gwalani, S. Gray, K. S. Han, T. A. Everett, T. A. Ajantiwalay, V. Murugesan, N. N. Rajput, V. G. Pol, *Nat. Commun.* **2023**, *14*, 868.
[36] D. Han, C. Cui, K. Zhang, Z. Wang, J. Gao, Y. Guo, Z. Zhang, S. Wu, L. Yin, Z. Weng, F. Kang, Q.-H. Yang, *Nat. Sustain.* **2021**, *5*, 205.
[37] X. Peng, T. Wang, B. Liu, Y. Li, T. Zhao, *Energy Environ. Sci.* **2022**, *15*, 5350.
[38] T. Wen, H. Xiao, S. Tan, X. Huang, B. Qu, L. Cao, G. Huang, J. Song, J. Wang, A. Tang, J. Yue, F. Pan, *J. Magnesium Alloys* **2024**, *12*, 2647.
[39] M. Li, X. Wang, J. Meng, C. Zuo, B. Wu, C. Li, W. Sun, L. Mai, *Adv. Mater.* **2024**, *36*, 2308628.
[40] C. Li, H. Xu, L. Ni, B. Qin, Y. Ma, H. Jiang, G. Xu, J. Zhao, G. Cui, *Adv. Energy Mater.* **2023**, *13*, 2301758.
[41] Z. Huang, Y. Hou, T. Wang, Y. Zhao, G. Liang, X. Li, Y. Guo, Q. i. Yang, Z. Chen, Q. Li, L. Ma, J. Fan, C. Zhi, *Nat. Commun.* **2021**, *12*, 3106.
[42] M. Okoshi, Y. Yamada, S. Komaba, A. Yamada, H. Nakai, *J. Electrochem. Soc.* **2017**, *164*, A54.
[43] T. Hosaka, K. Kubota, A. S. Hameed, S. Komaba, *Chem. Rev.* **2020**, *120*, 6358.
[44] M. Salama, I. Shterenberg, H. Gizbar, N. N. Eliaz, M. Kosa, K. Keinan-Adamsky, M. Afri, L. J. W. Shimon, H. E. Gottlieb, D. T. Major, Y. Gofer, D. Aurbach, *J. Phys. Chem.* **2016**, *120*, 19586.
[45] Y. Chen, N. R. Jaegers, H. Wang, K. S. Han, J. Z. Hu, K. T. Mueller, V. Murugesan, *J. Phys. Chem. Lett.* **2020**, *11*, 6443.
[46] D.-T. Nguyen, A. Y. S. Eng, R. Horia, Z. Sofer, A. D. Handoko, M.-F. Ng, Z. W. Seh, *Energy Storage Mater.* **2021**, *45*, 1120.
[47] R. Attias, M. Salama, B. Hirsch, Y. Goffer, D. Aurbach, *Joule* **2019**, *3*, 27.
[48] N. Sa, B. Pan, A. Saha-Shah, A. A. Hubaud, J. T. Vaughey, L. A. Baker, C. Liao, A. K. Burrell, *ACS Appl. Mater. Interfaces* **2016**, *8*, 16002.
[49] J. H. Connor, W. E. Reid, G. B. Wood, *J. Electrochem. Soc.* **1957**, *104*, 38.
[50] Y.-s. Guo, F. Zhang, J. Yang, F.-f. Wang, Y. NuLi, S.-i. Hirano, *Energy Environ. Sci.* **2012**, *5*, 9100.
[51] H. Dong, O. Tutusaus, Y. Liang, Y. Zhang, Z. Lebens-Higgins, W. Yang, R. Mohtadi, Y. Yao, *Nat. Energy* **2020**, *5*, 1043.
[52] J. Long, Y. Liu, Z. He, S. Tan, F. Xiong, H. Xu, W. Wang, G. Zhang, Z. Yang, Q. An, *ACS Nano* **2024**, *18*, 15239.
[53] D. Aurbach, M. Moshkovich, A. Schechter, R. Turgeman, *Electrochem. Solid-State Lett.* **2000**, *3*, 31.
[54] D. Y. Kim, Y. Lim, B. Roy, Y.-G. Ryu, S.-S. Lee, *Phys. Chem. Chem. Phys.* **2014**, *16*, 25789.

[55] S. Sakamoto, T. Imamoto, K. Yamaguchi, *Org. Lett.* **2001**, *3*, 1793.
[56] D. Aurbach, H. Gizbar, A. Schechter, O. Chusid, H. E. Gottlieb, Y. Gofer, I. Goldberg, *J. Electrochem. Soc.* **2002**, *149*, A115.
[57] Y. A. Wu, Z. Yin, M. Farmand, Y.-S. Yu, D. A. Shapiro, H.-G. Liao, W.-I. Liang, Y.-H. Chu, H. Zheng, *Sci. Rep.* **2017**, *7*, 42527.
[58] Y. Li, F. Wu, Y. Li, M. Liu, X. Feng, Y. Bai, C. Wu, *Chem. Soc. Rev.* **2022**, *51*, 4484.
[59] Y. Cheng, R. M. Stolley, K. S. Han, Y. Shao, B. W. Arey, N. M. Washton, K. T. Mueller, M. L. Helm, V. L. Sprenkle, J. Liu, G. Li, *Phys. Chem. Chem. Phys.* **2015**, *17*, 13307.
[60] Z. Liang, C. Ban, *Angew. Chem., Int. Ed.* **2021**, *60*, 11036.
[61] Z. Zhao-Karger, J. E. Mueller, X. Zhao, O. Fuhr, T. Jacob, M. Fichtner, *RSC Adv.* **2014**, *4*, 26924.
[62] W. Li, S. Cheng, J. Wang, Y. Qiu, Z. Zheng, H. Lin, S. Nanda, Q. Ma, Y. Xu, F. Ye, M. Liu, L. Zhou, Y. Zhang, *Angew. Chem., Int. Ed.* **2016**, *55*, 6406.
[63] Y. Xu, W. Li, G. Zhou, Z. Pan, Y. Zhang, *Energy Storage Mater.* **2018**, *14*, 253.
[64] K. A. See, K. W. Chapman, L. Zhu, K. M. Wiaderek, O. J. Borkiewicz, C. J. Barile, P. J. Chupas, A. A. Gewirth, *J. Am. Chem. Soc.* **2016**, *138*, 328.
[65] K. A. See, Y.-M. Liu, Y. Ha, C. J. Barile, A. A. Gewirth, *ACS Appl. Mater. Interfaces* **2017**, *9*, 35729.
[66] R. Attias, M. S. Chae, B. Dlugatch, M. Oliel, Y. Goffer, D. Aurbach, *ACS Catal.* **2020**, *10*, 7773.
[67] B. W. Schick, V. Vanoppen, M. Uhl, M. Kruck, S. Riedel, Z. Zhao-Karger, E. J. Berg, X. Hou, T. Jacob, *Angew. Chem., Int. Ed.* **2024**, *63*, 202413058.
[68] F. Xiong, Y. Fan, S. Tan, L. Zhou, Y. Xu, C. Pei, Q. An, L. Mai, *Nano Energy* **2018**, *47*, 210.
[69] Y. Liang, R. Feng, S. Yang, H. Ma, J. Liang, J. Chen, *Adv. Mater.* **2011**, *23*, 640.
[70] Z. Li, J. Häcker, M. Fichtner, Z. Zhao-Karger, *Adv. Energy Mater.* **2023**, *13*, 2300682.
[71] T. D. Gregory, R. J. Hoffman, R. C. Winterton, *J. Electrochem. Soc.* **1990**, *137*, 775.
[72] O. Mizrahi, N. Amir, E. Pollak, O. Chusid, V. Marks, H. Gottlieb, L. Larush, E. Zinigrad, D. Aurbach, *J. Electrochem. Soc.* **2008**, *155*, A103.
[73] N. Pour, Y. Gofer, D. T. Major, D. Aurbach, *J. Am. Chem. Soc.* **2011**, *133*, 6270.
[74] R. E. Doe, R. Han, J. Hwang, A. J. Gmitter, I. Shterenberg, H. D. Yoo, N. Pour, D. Aurbach, *Chem. Commun.* **2014**, *50*, 243.
[75] H. S. Kim, T. S. Arthur, G. D. Allred, J. Zajicek, J. G. Newman, A. E. Rodnyansky, A. G. Oliver, W. C. Boggess, J. Muldoon, *Nat. Commun.* **2011**, *2*, 427.
[76] Z. Zhao-Karger, X. Zhao, O. Fuhr, M. Fichtner, *RSC Adv.* **2013**, *3*, 16330.
[77] Z. Zhao-Karger, X. Zhao, D. Wang, T. Diemant, R. J. Behm, M. Fichtner, *Adv. Energy Mater.* **2014**, *5*, 1401155.
[78] E. G. Nelson, J. W. Kampf, B. M. Bartlett, *Chem. Commun.* **2014**, *50*, 5193.
[79] F.-F. Wang, Y.-S. Guo, J. Yang, Y. Nuli, S.-I. Hirano, *Chem. Commun.* **2012**, *48*, 10763.
[80] P. Liu, J. Long, R. Wang, Y. Zhou, B. Qu, L. Zhang, X. Zhou, Q. An, *Energy Storage Mater.* **2024**, *71*, 103679.
[81] J. T. Herb, C. Nist-Lund, J. Schwartz, C. B. Arnold, *ECS Electrochem. Lett.* **2015**, *4*, A49.
[82] J. T. Herb, C. A. Nist-Lund, C. B. Arnold, *J. Mater. Chem. A* **2017**, *5*, 7801.
[83] M. Cheng, Y. Wang, D. Zhang, S. Zhang, Y. Yang, X. Lv, J. Wang, Y. NuLi, *J. Energy Chem.* **2023**, *76*, 1.
[84] J. T. Herb, C. A. Nist-Lund, C. B. Arnold, *ACS Energy Lett.* **2016**, *1*, 1227.
[85] R. N. Samajdar, S. Marchesini, S. A. Brown, S. D. Robertson, K. R. Paton, A. J. Pollard, A. J. Wain, *ACS Energy Lett.* **2023**, *8*, 1864.
[86] T. Liu, Y. Shao, G. Li, M. Gu, J. Hu, S. Xu, Z. Nie, X. Chen, C. Wang, J. Liu, *J. Mater. Chem. A* **2014**, *2*, 3430.
[87] E. G. Nelson, S. I. Brody, J. W. Kampf, B. M. Bartlett, *J. Mater. Chem. A* **2014**, *2*, 18194.
[88] C. J. Barile, E. C. Barile, K. R. Zavadil, R. G. Nuzzo, A. A. Gewirth, *J. Phys. Chem.* **2014**, *118*, 27623.
[89] J. Luo, S. He, T. L. Liu, *ACS Energy Lett.* **2017**, *2*, 1197.
[90] P. Canepa, S. Jayaraman, L. Cheng, N. N. Rajput, W. D. Richards, G. S. Gautam, L. A. Curtiss, K. A. Persson, G. Ceder, *Energy Environ. Sci.* **2015**, *8*, 3718.
[91] N. R. Park, M. Zhang, B. Han, W. Li, K. Qian, H. Nguyen, S. Kumakura, Y. S. Meng, *Adv. Energy Mater.* **2024**, *14*, 2401968.
[92] M. Mao, X. Ji, Q. Wang, Z. Lin, M. Li, T. Liu, C. Wang, Y.-S. Hu, H. Li, X. Huang, L. Chen, L. Suo, *Nat. Commun.* **2023**, *14*, 1082.
[93] Y. Guo, F. Zhang, J. Yang, F. Wang, *Electrochem. Commun.* **2012**, *18*, 24.
[94] J. Zhu, Y. Guo, J. Yang, Y. Nuli, F. Zhang, J. Wang, S.-I. Hirano, *J. Power Sources* **2014**, *248*, 690.
[95] J. Long, Y. An, Z. Yang, G. Zhang, J. Zhang, S. Tan, Q. An, *Chem. Eng. J.* **2023**, *461*, 141901.
[96] H. Xu, Z. Zhang, Z. Cui, A. Du, C. Lu, S. Dong, J. Ma, X. Zhou, G. Cui, *Electrochem. Commun.* **2017**, *83*, 72.
[97] Z. Zhang, Z. Cui, L. Qiao, J. Guan, H. Xu, X. Wang, P. Hu, H. Du, S. Li, X. Zhou, S. Dong, Z. Liu, G. Cui, L. Chen, *Adv. Energy Mater.* **2017**, *7*, 1602055.
[98] H. Xu, Z. Zhang, J. Li, L. Qiao, C. Lu, K. Tang, S. Dong, J. Ma, Y. Liu, X. Zhou, G. Cui, *ACS Appl. Mater. Interfaces* **2018**, *10*, 23757.
[99] A. Du, Z. Zhang, H. Qu, Z. Cui, L. Qiao, L. Wang, J. Chai, T. Lu, S. Dong, T. Dong, H. Xu, X. Zhou, G. Cui, *Energy Environ. Sci.* **2017**, *10*, 2616.
[100] X. Song, J. Sun, W. Ren, L. Wang, B. Yang, H. Ning, P. Zhang, Z. Caixiang, Z. Tie, X. Zhang, Y. NuLi, Z. Jin, *Angew. Chem., Int. Ed.* **2024**, *64*, 202417450.
[101] M. Cheng, W. Ren, D. Zhang, S. Zhang, Y. Yang, X. Lv, J. Yang, J. Wang, Y. NuLi, *Energy Storage Mater.* **2022**, *51*, 764.
[102] X. Huang, J. Wen, J. Lei, G. Huang, F. Pan, L. Li, *ACS Appl. Mater. Interfaces* **2022**, *14*, 8906.
[103] J. H. Ha, J. Cho, J. H. Kim, B. W. Cho, H. C. Ham, S. H. Oh, *J. Power Sources* **2018**, *398*, 120.
[104] J. H. Ha, B. Adams, J.-H. Cho, V. Duffort, J. H. Kim, K. Y. Chung, B. W. Cho, L. F. Nazar, S. H. Oh, *J. Mater. Chem. A* **2016**, *4*, 7160.
[105] G. Yang, Y. Li, C. Zhang, J. Wang, Y. Bai, C. Y. J. Lim, M.-F. Ng, Z. Chang, S. Kumar, Z. Sofer, W. Liu, Z. W. Seh, *Nano Lett.* **2022**, *22*, 9138.
[106] R. Li, R. Zhang, Q. Liu, J. An, Y. Song, B. Deng, Y. Ma, H. Huo, Y. Gao, J. Wang, P. Zuo, G. Yin, *Chem. Eng. J.* **2023**, *462*, 141998.
[107] R. Mohtadi, M. Matsui, T. S. Arthur, S.-J. Hwang, *Angew. Chem., Int. Ed.* **2012**, *51*, 9780.
[108] Y. Shao, T. Liu, G. Li, M. Gu, Z. Nie, M. Engelhard, J. Xiao, D. Lv, C. Wang, J. i.-G. Zhang, J. Liu, *Sci. Rep.* **2013**, *3*, 3130.
[109] J. Chang, R. T. Haasch, J. Kim, T. Spila, P. V. Braun, A. A. Gewirth, R. G. Nuzzo, *ACS Appl. Mater. Interfaces* **2015**, *7*, 2494.
[110] H. Fan, Z. Zheng, L. Zhao, W. Li, J. Wang, M. Dai, Y. Zhao, J. Xiao, G. Wang, X. Ding, H. Xiao, J. Li, Y. Wu, Y. Zhang, *Adv. Funct. Mater.* **2020**, *30*, 1909370.
[111] H. Fan, X. Zhang, J. Xiao, Y. Lin, S. Ren, Y. Zhao, H. Yuan, L. Pan, Q. Lin, H. Liu, Y. Su, Y. Su, Y. Liu, Y. Zhang, *Energy Storage Mater.* **2022**, *51*, 873.
[112] D. Zhang, M. Liu, J. Ma, K. Yang, Z. Chen, K. Li, C. Zhang, Y. Wei, M. Zhou, P. Wang, Y. He, W. Lv, Q.-H. Yang, F. Kang, Y.-B. He, *Nat. Commun.* **2022**, *13*, 6966.

[113] F. Wang, H. Hua, Y. Zhuang, J. Wu, J. Zeng, J. Zhao, *Adv. Funct. Mater.* **2025**, *35*, 2414181.
[114] W. Si, M. Tian, Z. Wang, H. Ma, Y. Du, W. Wang, W. Zhang, H. Y. Yang, S. Chen, *Adv. Funct. Mater.* **2025**, *35*, 2411881.
[115] A. Roy, M. Sotoudeh, S. Dinda, Y. Tang, C. Kübel, A. Groß, Z. Zhao-Karger, M. Fichtner, Z. Li, *Nat. Commun.* **2024**, *15*, 492.
[116] I. Shterenberg, M. Salama, H. D. Yoo, Y. Gofer, J.-B. Park, Y.-K. Sun, D. Aurbach, *J. Electrochem. Soc.* **2015**, *162*, A7118.
[117] T. Gao, S. Hou, F. Wang, Z. Ma, X. Li, K. Xu, C. Wang, *Angew. Chem., Int. Ed.* **2017**, *56*, 13526.
[118] X. Ren, D. Tao, Y. Tang, Y. Cao, F. Xu, *J. Mater. Chem. A* **2023**, *11*, 9955.
[119] S. Cui, T. Li, D. Tao, D. Zhang, Y. Cao, F. Xu, *ACS Mater. Lett.* **2024**, *6*, 1883.
[120] D. Chen, D. Tao, X. Ren, F. Wen, T. Li, Z. Chen, Y. Cao, F. Xu, *ACS Nano* **2022**, *16*, 20510.
[121] Y. He, Q. i. Li, L. Yang, C. Yang, D. Xu, *Angew. Chem., Int. Ed.* **2019**, *58*, 7615.
[122] J. Xiao, X. Zhang, H. Fan, Y. Zhao, Y. i. Su, H. Liu, X. Li, Y. Su, H. Yuan, T. Pan, Q. Lin, L. Pan, Y. Zhang, *Adv. Mater.* **2022**, *34*, 2203783.
[123] D.-T. Nguyen, A. Y. S. Eng, M.-F. Ng, V. Kumar, Z. Sofer, A. D. Handoko, G. S. Subramanian, Z. W. Seh, *Cell Reports Physical Science* **2020**, *1*, 100265.
[124] D. Chinnadurai, W. Y. Lieu, S. Kumar, G. Yang, Y. Li, Z. W. Seh, *Nano Lett.* **2023**, *23*, 1564.
[125] C. Liao, N. Sa, B. Key, A. K. Burrell, L. Cheng, L. A. Curtiss, J. T. Vaughey, J.-J. Woo, L. Hu, B. Pan, Z. Zhang, *J. Mater. Chem. A* **2015**, *3*, 6082.
[126] Y. Yang, Y. Qiu, Y. NuLi, W. Wang, J. Yang, J. Wang, *J. Mater. Chem. A* **2019**, *7*, 18295.
[127] J. Long, Y. Liu, W. Zhang, G. Zhang, P. Liu, L. Cui, C. Zhou, J. Ren, Z. He, Q. An, L. Mai, *ACS Energy Lett.* **2024**, *9*, 5019.
[128] H. Dong, Y. Liang, O. Tutusaus, R. Mohtadi, Y. Zhang, F. Hao, Y. Yao, *Joule* **2019**, *3*, 782.
[129] L. Zhou, Q. Liu, Z. Zhang, K. Zhang, F. Xiong, S. Tan, Q. An, Y.-M. Kang, Z. Zhou, L. Mai, *Adv. Mater.* **2018**, *30*, 1801984.
[130] Y. Chen, R. Atwi, D. T. Nguyen, J. D. Bazak, N. T. Hahn, J. Ryu, J. A. Sears, K. S. Han, M. Song, Z. Li, A. J. Karkamkar, J. Z. Hu, K. R. Zavadil, N. N. Rajput, K. T. Mueller, V. Murugesan, *J. Am. Chem. Soc.* **2024**, *146*, 12984.
[131] Y. Yang, J. Wang, X. Du, H. Jiang, A. Du, X. Ge, N. Li, H. Wang, Y. Zhang, Z. Chen, J. Zhao, G. Cui, *J. Am. Chem. Soc.* **2023**, *145*, 12093.
[132] G. A. Giffin, A. Moretti, S. Jeong, S. Passerini, *J. Phys. Chem. C* **2014**, *118*, 9966.
[133] N. N. Rajput, X. Qu, N. Sa, A. K. Burrell, K. A. Persson, *J. Am. Chem. Soc.* **2015**, *137*, 3411.
[134] V. Prabhakaran, G. Agarwal, J. D. Howard, J. Zajicek, G. D. Allred, W. C. BoggessS, Wi, V. Shutthanandan, D.-T. Nguyen, L. Soule, G. E. Johnson, Y.-S. Liu, F. Yang, X. Feng, J. Guo, K. Hankins, L. A. Curtiss, K. T. Mueller, R. S. Assary, V. Murugesan, *ACS Appl. Mater. Interfaces* **2023**, *15*, 7518.
[135] D. Aurbach, I. Weissman, Y. Gofer, E. Levi, *Chem. Rec.* **2003**, *3*, 61.
[136] J. Muldoon, C. B. Bucur, A. G. Oliver, J. Zajicek, G. D. Allred, W. C. Boggess, *Energy Environ. Sci.* **2013**, 482.
[137] Z. Zhao-Karger, M. E. Gil Bardaji, O. Fuhr, M. Fichtner, *J. Mater. Chem. A* **2017**, *5*, 10815.
[138] Z. Zhao-Karger, R. Liu, W. Dai, Z. Li, T. Diemant, B. P. Vinayan, C. Bonatto Minella, X. Yu, A. Manthiram, R. J. Behm, M. Ruben, M. Fichtner, *ACS Energy Lett.* **2018**, *3*, 2005.
[139] T. Mandai, *ACS Appl. Mater. Interfaces* **2020**, *12*, 39135.
[140] G. Wang, X. Liu, H. Shi, Y. Ma, Z. Wang, C. Sun, F. Song, Z. Zhang, S. Dong, M. Sun, A. Du, G. Cui, *ACS Energy Lett.* **2024**, *9*, 48.
[141] Y. Zhang, J. Li, W. Zhao, H. Dou, X. Zhao, Y. Liu, B. Zhang, X. Yang, *Adv. Mater.* **2022**, *34*, 2108114.
[142] B. Dlugatch, M. Mohankumar, R. Attias, B. M. Krishna, Y. Elias, Y. Gofer, D. Zitoun, D. Aurbach, *ACS Appl. Mater. Interfaces* **2021**, *13*, 54894.
[143] Z. Li, T. Diemant, Z. Meng, Y. Xiu, A. Reupert, L. Wang, M. Fichtner, *ACS Appl. Mater. Interfaces* **2021**, *13*, 33123.
[144] R. Horia, D.-T. Nguyen, A. Y. S. Eng, Z. W. Seh, *Nano Lett.* **2021**, *21*, 8220.
[145] S. Li, J. Zhang, S. Zhang, Q. Liu, H. Cheng, L. Fan, W. Zhang, X. Wang, Q. Wu, Y. Lu, *Nat. Energy* **2024**, *9*, 285.
[146] T. Pavčnik, J. Imperl, M. Kolar, R. Dominko, J. Bitenc, *J. Mater. Chem. A* **2024**, *12*, 3386.
[147] J. Luo, Y. Bi, L. Zhang, X. Zhang, T. L. Liu, *Angew. Chem., Int. Ed.* **2019**, *58*, 6967.
[148] W. Ren, D. Wu, Y. NuLi, D. Zhang, Y. Yang, Y. Wang, J. Yang, J. Wang, *ACS Energy Lett.* **2021**, *6*, 3212.
[149] X. Huang, S. Tan, J. Chen, Z. Que, R. Deng, J. Long, F. Xiong, G. Huang, X. Zhou, L. Li, J. Wang, L. Mai, F. Pan, *Adv. Funct. Mater.* **2024**, *34*, 2314146.
[150] E. N. Keyzer, J. Lee, Z. Liu, A. D. Bond, D. S. Wright, C. P. Grey, *J. Mater. Chem. A* **2019**, *7*, 2677.
[151] K. a.-C. Lau, T. J. Seguin, E. V. Carino, N. T. Hahn, J. G. Connell, B. J. Ingram, K. A. Persson, K. R. Zavadil, C. Liao, *J. Electrochem. Soc.* **2019**, *166*, A1510.
[152] T. Pavčnik, M. Radi, O. Lužanin, R. Dedryvère, D. S. Tchitchekova, A. Ponrouch, J. Bitenc, R. Dominko, *J. Power Sources* **2025**, *626*, 235711.
[153] D. Wang, X. Du, G. Chen, F. Song, J. Du, J. Zhao, Y. Ma, J. Wang, A. Du, Z. Cui, X. Zhou, G. Cui, *Angew. Chem., Int. Ed.* **2023**, *62*, 202217709.
[154] A. Schmidt, H. Koger, A. Barthélemy, G. Studer, B. Esser, I. Krossing, *Batteries Supercaps* **2022**, *5*, 202200340.
[155] P. Jankowski, Z. Li, Z. Zhao-Karger, T. Diemant, M. Fichtner, T. Vegge, J. M. G. Lastra, *Energy Storage Mater.* **2022**, *45*, 1133.
[156] T. J. Carter, R. Mohtadi, T. S. Arthur, F. Mizuno, R. Zhang, S. Shirai, J. W. Kampf, *Angew. Chem., Int. Ed.* **2014**, *53*, 3173.
[157] O. Tutusaus, R. Mohtadi, T. S. Arthur, F. Mizuno, E. G. Nelson, Y. V. Sevryugina, *Angew. Chem., Int. Ed.* **2015**, *54*, 7900.
[158] S. G. McArthur, R. Jay, L. Geng, J. Guo, V. Lavallo, *Chem. Commun.* **2017**, *53*, 4453.
[159] N. T. Hahn, T. J. Seguin, K.-C. Lau, C. Liao, B. J. Ingram, K. A. Persson, K. R. Zavadil, *J. Am. Chem. Soc.* **2018**, *140*, 11076.
[160] M. Watanabe, J. Kanazawa, T. Hamamura, T. Shimokawa, K. Miyamoto, M. Hibino, K. Nakura, Y. Inatomi, Y. Kitazawa, M. Uchiyama, *Mater. Adv.* **2021**, *2*, 937.
[161] A. W. Tomich, J. Chen, V. Carta, J. Guo, V. Lavallo, *ACS Cent. Sci.* **2024**, *10*, 264.
[162] S. G. McArthur, L. Geng, J. Guo, V. Lavallo, *Inorg. Chem. Front.* **2015**, *2*, 1101.
[163] S. Körbe, P. J. Schreiber, J. Michl, *Chem. Rev.* **2006**, *106*, 5208.
[164] H. Luo, X. Ji, B. Zhang, M. Chen, X. Wu, Y. Zhu, X. Yu, J. Wang, H. Zhang, Y. Hong, Y. Zou, G. Feng, Y. Qiao, H. Zhou, S.-G. Sun, *Angew. Chem., Int. Ed.* **2024**, *63*, 202412214.
[165] W. Xu, J. Li, X. Liao, L. Zhang, X. Zhang, C. Liu, K. Amine, K. Zhao, J. Lu, *J. Am. Chem. Soc.* **2023**, *145*, 22456.
[166] N. T. Hahn, E. P. Kamphaus, Y. Chen, V. Murugesan, K. T. Mueller, L. Cheng, K. R. Zavadil, *ACS Appl. Energy Mater.* **2023**, *6*, 3264.
[167] S. Fan, G. M. Asselin, B. Pan, H. Wang, Y. Ren, J. T. Vaughey, N. Sa, *ACS Appl. Mater. Interfaces* **2020**, *12*, 10252.
[168] S. Hou, X. Ji, K. Gaskell, P.-F. Wang, L. Wang, J. Xu, R. Sun, O. Borodin, C. Wang, *Science* **2021**, *374*, 172.
[169] F. Wang, H. Hua, D. Wu, J. Li, Y. Xu, X. Nie, Y. Zhuang, J. Zeng, J. Zhao, *ACS Energy Lett.* **2023**, *8*, 780.
[170] Y. Du, Y. Chen, S. Tan, J. Chen, X. Huang, L. Cui, J. Long, Z. Wang, X. Yao, B. Shang, G. Huang, X. Zhou, L. Li, J. Wang, F. Pan, *Energy Storage Mater.* **2023**, *62*, 102939.

[171] D. Zhang, Y. Wang, Y. Yang, Y. Zhang, Y. Zhao, M. Pan, Y. Sun, S. Chen, X. Liu, J. Wang, Y. NuLi, *Adv. Energy Mater.* **2023**, *13*, 2301795.
[172] W. Wang, S. Ju, H. Zhang, X. Zhou, X. Yu, *Energy Storage Mater.* **2024**, *70*, 103493.
[173] J. Zhang, J. Liu, M. Wang, Z. Zhang, Z. Zhou, X. Chen, A. Du, S. Dong, Z. Li, G. Li, G. Cui, *Energy Environ. Sci.* **2023**, *16*, 1111.
[174] M. Wang, W. Sun, K. Zhang, Z. Zhang, A. Du, S. Dong, J. Zhang, J. Liu, X. Chen, Z. Zhou, F. Li, Z. Li, G. Li, G. Cui, *Energy Environ. Sci.* **2024**, *17*, 630.
[175] C. Li, W. Sun, H. Zhou, K. Xun, H. Cao, Z. Zhang, Z. Zhou, J. Liu, G. Li, *Adv. Funct. Mater.* **2025**, *35*, 2417287.
[176] W. Zhao, Z. Pan, Y. Zhang, Y. Liu, H. Dou, Y. Shi, Z. Zuo, B. Zhang, J. Chen, X. Zhao, X. Yang, *Angew. Chem., Int. Ed.* **2022**, *61*, 202205187.
[177] S. Wang, K. Wang, Y. Zhang, Y. Jie, X. Li, Y. Pan, X. Gao, Q. Nian, R. Cao, Q. Li, S. Jiao, D. Xu, *Angew. Chem., Int. Ed.* **2023**, *62*, 202304411.
[178] Z. Fan, W. Zhao, S. Shi, M. Zhou, J. Li, Y. Liu, Z. Pan, X. Yang, *Angew. Chem., Int. Ed.* **2024**, *64*, 202416582.
[179] C. Li, R. D. Guha, A. Shyamsunder, K. A. Persson, L. F. Nazar, *Energy Environ. Sci.* **2024**, *17*, 190.
[180] J. Xiao, X. Zhang, H. Fan, Q. Lin, Z. S. Ng, W. Chen, Y. Zhang, *ACS Appl. Mater. Interfaces* **2024**, *16*, 7673.
[181] Y. Sun, Y. Wang, L. Jiang, D. Dong, W. Wang, J. Fan, Y.-C. Lu, *Energy Environ. Sci.* **2023**, *16*, 265.
[182] C. Chen, J. Chen, S. Tan, Z. Gao, X. Huang, Z. He, J. Huang, R. Deng, F. Xiong, G. Huang, J. Wang, L. Li, F. Pan, *Adv. Funct. Mater.* **2025**, 2505843.
[183] C. Chen, J. Chen, S. Tan, X. Huang, Y. Du, B. Shang, B. Qu, G. Huang, X. Zhou, J. Wang, L. Li, F. Pan, *Energy Storage Mater.* **2023**, *59*, 102792.
[184] J. Xiao, X. Zhang, H. Fan, Q. Lin, L. Pan, H. Liu, Y. Su, X. Li, Y. Su, S. Ren, Y. Lin, Y. Zhang, *Adv. Energy Mater.* **2022**, *12*, 2202602.
[185] S. Ilic, S. N. Lavan, N. J. Leon, H. Liu, A. Jain, B. Key, R. S. Assary, C. Liao, J. G. Connell, *ACS Appl. Mater. Interfaces* **2023**, *16*, 435.
[186] H. Wang, X. Feng, Y. Chen, Y. i.-S. Liu, K. S. Han, M. Zhou, M. H. Engelhard, V. Murugesan, R. S. Assary, T. L. Liu, W. Henderson, Z. Nie, M. Gu, J. Xiao, C. Wang, K. Persson, D. Mei, J. i.-G. Zhang, K. T. Mueller, J. Guo, K. Zavadil, Y. Shao, J. Liu, *ACS Energy Lett.* **2020**, *5*, 200.
[187] J. Long, S. Tan, J. Wang, F. Xiong, L. Cui, Q. An, L. Mai, *Angew. Chem., Int. Ed.* **2023**, *62*, 202301934.
[188] Y. Shen, Y. Wang, Y. Miao, Q. Li, X. Zhao, X. Shen, *Adv. Mater.* **2023**, *35*, 2208289.
[189] C. Li, R. D. Guha, S. D. House, J. D. Bazak, Y. Yu, L. Zhou, K. Zavadil, K. A. Persson, L. F. Nazar, *Joule* **2024**, *9*, 101790.
[190] Z. Li, D.-T. Nguyen, J. D. Bazak, K. S. Han, Y. Chen, V. Prabhakaran, T. T. Le, Z. Cheng, M. Song, V. G. Pol, K. T. Mueller, V. Murugesan, *Adv. Energy Mater.* **2024**, *14*, 2301544.
[191] M. Zhang, W. Zhao, Y. Liu, M. Zhou, Z. Pan, X. Yang, *ACS Energy Lett.* **2025**, *10*, 552.
[192] D. Zhang, M. Zhou, E. Sheha, J. Wang, J. Yang, Y. NuLi, *Nano Lett.* **2025**, *25*, 4846.
[193] T. Wang, K. Chen, G. Li, Z. Chen, Y. Gao, C. Li, *ACS Nano* **2025**, *19*, 16877.
[194] G. Yang, Y. Li, J. Wang, Y. Lum, C. Y. J. Lim, M.-F. Ng, C. Zhang, Z. Chang, Z. Zhang, A. D. Handoko, T. Ghosh, S. Li, Z. Sofer, W. Liu, Y. Yao, Z. W. Seh, *Energy Environ. Sci.* **2024**, *17*, 1141.
[195] D. Chinnadurai, Y. Li, C. Zhang, G. Yang, W. Y. Lieu, S. Kumar, Z. Xing, W. Liu, Z. W. Seh, *Nano Lett.* **2023**, *23*, 11233.
[196] A. L. Lipson, S.-D. Han, B. Pan, K. A. See, A. A. Gewirth, C. Liao, J. T. Vaughey, B. J. Ingram, *J. Electrochem. Soc.* **2016**, *163*, A2253.
[197] J. Xu, V. Koverga, A. Phan, A. min Li, N. Zhang, M. Baek, C. Jayawardana, B. L. Lucht, A. T. Ngo, C. Wang, *Adv. Mater.* **2024**, *36*, 2306462.
[198] K. Tang, A. Du, X. Du, S. Dong, C. Lu, Z. Cui, L. Li, G. Ding, F. Chen, X. Zhou, G. Cui, *Small* **2020**, *16*, 2005424.
[199] Y. Wang, Z. Li, Y. Hou, Z. Hao, Q. Zhang, Y. Ni, Y. Lu, Z. Yan, K. Zhang, Q. Zhao, F. Li, J. Chen, *Chem. Soc. Rev.* **2023**, *52*, 2713.
[200] T. Wang, X. Zhao, F. Liu, L. i.-Z. Fan, *J. Energy Chem.* **2021**, *59*, 608.
[201] R. Li, W. Zhao, Z. Fan, M. Zhang, J. Li, R. Li, Z. Zuo, X. Yang, *Energy Environ. Sci.* **2025**, *18*, 6790.

Juncai Long received his Ph.D. degree from Wuhan University of Technology in 2025. His research currently centers on the rational design of electrolytes/organic electrode materials for magnesium-ion batteries and in situ/ex situ characterization of electrochemical reaction.

Shuangshuang Tan is currently an associate professor at the College of Materials Science and Engineering, Chongqing University. He received his Ph.D. degree from Wuhan University of Technology in 2021. His current research focuses on magnesium battery electrode materials and electrolytes, energy storage materials, and devices.

Qinyou An is Professor of Materials Science and Engineering at Wuhan University of Technology (WUT). He received his Ph.D. degree from WUT in 2014. He carried out his postdoctoral research in the laboratory of Prof. Yan Yao at the University of Houston in 2014–2015. His current research focuses on multivalent ion batteries, including magnesium-ion, calcium-ion, and zinc-ion batteries.

Liqiang Mai is Chair Professor and Vice-President of Wuhan University of Technology (WUT), and Fellow of the Royal Society of Chemistry. He received his Ph.D. from WUT in 2004 and carried out his postdoctoral research at the Georgia Institute of Technology in 2006–2007. He worked as an advanced research scholar at Harvard University from 2008–2011 and University of California, Berkeley in 2017. His current research interests focus on new nanomaterials for electrochemical energy storage and micro/nano energy devices.